

TOPICS IN PERTURBATIVE FIELD THEORY

Thesis by

Anthony Emerson Terrano

In Partial Fulfillment of the Requirements

for the Degree of

Doctor of Philosophy

California Institute of Technology

Pasadena, California

1981

(Submitted May 13, 1981)

Acknowledgements

I am grateful to my advisor M. Gell-Mann for discussions and encouragement. I owe a profound debt to my collaborators -- R. K. Ellis, D. A. Ross, and S. Wolfram -- for their patience and encouragement. I am grateful to many people for discussions; in particular: S. Brodsky, W. Celmaster, G. C. Fox, T. D. Gottschalk, J. A. Harvey, and D. B. Reiss. Finally, I want to thank B. H. Cooper, J. A. Harvey, D. B. Reiss, and S. Wolfram for their advice and support during the last few years.

Abstract

This thesis discusses several results in perturbative field theory. The first two sections present a calculation of the order α_s^2 corrections to the event shape in e^+e^- annihilation into hadrons. A technique for the calculation of Feynman diagrams based upon a generalization of the multipole expansion of a potential is discussed in the third section. Computer programs which can be used evaluate the traces which arise in the evaluation of Feynman diagrams are described in an Appendix.

Table of Contents

1. Introduction
 2. Shapes of Three and Four Jet Events in e^+e^- Annihilation
 3. Perturbative Evaluation of Event Shapes in e^+e^- Annihilation
 4. A Method of Feynman Diagram Evaluation
- Appendix: On the evaluation of gamma matrix traces by computer

The first two papers in this thesis concern the investigation of quantum chromodynamics (QCD) through the use of perturbation theory. QCD is presently believed to provide a correct description of hadronic interactions [1]. Studied perturbatively, the interaction between the elementary quanta in QCD is found to be small when the energies involved are large relative to hadronic masses, and to diverge for smaller energies [2]. These results are the theoretical reflections of the observed approximate scaling in high energy lepton-hadron interactions on the one hand and confinement of quarks and gluons inside hadrons on the other. The scale dependence of the strength of the interaction in QCD may be absorbed into an energy-dependent effective coupling [2,3]. A typical high-energy hadronic interaction may be broken into three phases. In the initial phase the incident hadrons are resolved into their constituents; in the middle phase these quarks and gluons interact sufficiently energetically that perturbation theory may be used to calculate the outcome of their scattering; and in the final phase the scattered quanta combine to form hadrons. Although the initial and final processes lie beyond the perturbative regime and are presently incalculable, it is believed to be possible to isolate their effects in a universal manner, leaving a finite, calculable, perturbative kernel [4]. Thus, by studying features of hadronic interactions which are sensitive to the structure of events only at short distances, useful results may be obtained from QCD using perturbation theory.

High energy e^+e^- annihilation into hadrons is probably the simplest process to analyze in QCD since the initial state does not contain any quarks or gluons. At intermediate center of mass energies, the perturbative final state consists of a quark and an anti-quark. Each particle then

evolves into a shower of hadrons whose directions of motion are collimated. At sufficiently large energies, the observed final states are indeed approximately collinear: they consist of two jets of hadrons. At greater center of mass energies, one of the quarks may radiate an energetic gluon while still in the perturbative regime. If this gluon has sufficiently high transverse momentum to escape the quarks, it may evolve into a third jet. The rate at which three jet final states occur [5] is therefore proportional to the coupling α_s between quarks and gluons. However, the scale at which α_s acts, and consequently the magnitude of α_s , cannot be determined from the lowest order calculation alone. A change in the scale of α_s is formally of order α_s^2 and can be made consistently only if all of the order α_s^2 corrections are also known. The first radiative correction to the acollinearity distribution is given in the first paper in this thesis. For any definition of a three jet event, the three jet rate can be found from this distribution. The qualitative result is independent of the precise definition, however: the corrections are large. The implications of this result for the reliability of perturbation theory are also discussed in paper 1.

The details of this calculation are presented in paper 2 of this thesis. The n-dimensional gamma matrix algebra required in the evaluation of the diagrams was performed using computer programs developed here. The programs are described briefly in an appendix.

After this calculation was completed, several other workers studied the same process. The thrust distribution has been calculated using our result for the unintegrated cross section; the corrections to it are also found to be large [6]. Two other groups have repeated the entire calculation, each using a different method for isolating the infra-red divergences

in each diagram and showing that they vanish when added together. Both methods are distinct from the one which we employed. One of the groups also finds large corrections to both the thrust distribution and the acollinearity [7]. The second group has found much smaller corrections to the thrust distribution [8]. Since the quantities computed by the various groups are different, the possibility remains that all results are correct. All groups have obtained the same result for the unintegrated cross section.

The third paper of this thesis presents a new method for evaluating the divergent integrals which arise in Feynman diagram calculations. The integrands are invariant functions of the momenta of the real and virtual particles in the diagram. Each factor in the denominator is just the propagator of a spinless particle, i.e. the Fourier transform of a radial potential. When the integrals are dimensionally regularized, the integration variables are the N -dimensional momenta of the virtual particles. In the usual procedure, explicit covariance is maintained at each step of the calculation. This leads, in the multiloop case, to subsidiary integrals which in general can be evaluated only numerically. It is of great interest however to have an analytic expression for these integrals. With such expressions, the origin of large constant terms may be investigated. For many integrals, if a particular Lorentz frame is chosen and each propagator is expanded in multipole moments around the chosen center, the integrals which result are straightforward to evaluate. Since the potential is spherically symmetric, the different moments are not coupled and the angular integration is replaced by a sum over the moments. In order for this method to be of practical use, the moments must be found in an indefinite number of dimensions so that the divergences of

perturbation theory can be controlled. The expansions in paper 3 have been used to calculate the three-loop charge renormalization effects due to quartic scalar interactions in general gauge theories [9].

REFERENCES for the introduction

1. H. D. Politzer, Phys. Rep. 14C (1974); R. D. Field, Proc. La Jolla Summer School (1978)
2. H. D. Politzer, Phys. Rev. Lett. 30 (1974) 1346; D. Gross and F. Wilczek, *ibid.* (1974) 1343
3. M. Gell-Mann and F. Low, Phys. Rev. 95 (1954) 1300
4. R. K. Ellis et al., Nucl. Phys. B152 (1979) 129
5. J. Ellis, M. K. Gaillard, and G. G. Ross, Nucl. Phys. B111 (1976) 253; G. C. Fox and S. Wolfram, Phys. Rev. Lett. 41 (1978) 1581
6. Z. Kunst DESY report DESY 80/79 (1980)
7. K. J. F. Gaemers, S. J. Oldham, and J. A. M. Vermaseren CERN preprint TH.3002-CERN (1980)
8. F. Fabricius, I. Schmitt, G. Scheirholz, and G. Kramer DESY report DESY 80/91 (1980)
9. D. R. T. Jones, Phys. Rev. D22 (1980) 3140

2. Shapes of Three and Four Jet Events in e^+e^- Annihilation

Shapes of Three and Four Jet Events in e^+e^- Annihilation

R. K. Ellis*, D. A. Ross**, and A. E. Terrano
 California Institute of Technology, Pasadena, California 91125

Presented by A. E. Terrano

In this talk I describe the results of the calculation of event shapes in e^+e^- annihilation to order α_s^2 (details and complete references have been presented elsewhere¹). Our results are presented in terms of the tensor

$$\theta^{ij} = \sum_a \frac{p_a^i p_a^j}{|P_a|} \sum_a |P_a| \quad ,$$

where P_a^i are the components of the center of mass three-momentum of hadron a and the sum runs over all hadrons. Since this tensor combines parallel momenta linearly, it is infra-red finite and calculable in perturbation theory. The eigenvalues of θ are determined by the characteristic equation

$$\lambda^3 - \lambda^2 + \frac{C}{3}\lambda - \frac{D}{27} = 0; \quad 0 \leq C, D \leq 1 \quad .$$

The quantities C and D are symmetric functions of the eigenvalues

$$C = 3(\lambda_1\lambda_2 + \lambda_2\lambda_3 + \lambda_3\lambda_1), \quad D = 27(\lambda_1\lambda_2\lambda_3) \quad ,$$

and provide a convenient measure of the shape of the event. Since the tensor has unit trace, the distribution in the eigenvalues is fully determined by the distribution in C and D .

In QCD perturbation theory we can define an analogous tensor $\bar{\theta}$ by replacing the observed hadron momenta P by the parton momenta p . These two tensors are equal up to hadronization corrections which vanish like inverse powers of the total center of mass energy Q , but which at present energies play a significant role in the determination of the shape of the hadronic events. We have calculated the properties of θ for massless quarks and gluons in QCD and have taken no account of the effects of hadronization. Nevertheless, our calculation is a prerequisite for a more complete analysis.

For a two jet final state, only one of the eigenvalues of $\bar{\theta}$ will be nonzero, and both C and D will vanish; for a three jet final state, two of the eigenvalues will be nonzero with the result that C lies between 0 and .75 while D vanishes. Thus C measures the acollinearity of an event and D measures its acoplanarity.

Invited talk presented at XXth Int. Conf. on High Energy Physics, Madison, Wisc. (1980)

In Fig. 1 we display $\frac{C}{\sigma_0} \frac{d\sigma}{dC}$ in units of $\frac{\alpha_s}{2\pi}$ for the process $e^+e^- \rightarrow q\bar{q}G$ in the Born approximation. The distribution is completely specified by adding a term proportional to $\delta(C)$ such that the total cross-section is equal to $\sigma = \sigma_0(1 + \alpha_s/\pi)$. The determination of

the $O(\alpha_s^2)$ correction to the distribution in Fig. 1 requires the calculation (for $C \neq 0$) of the cross-sections for $e^+e^- \rightarrow q\bar{q}GG$ and $q\bar{q}q\bar{q}$ in the Born approximation and $e^+e^- \rightarrow q\bar{q}G$ to one loop. The ultraviolet divergences are controlled using dimensional regularization and renormalization is performed according to the \overline{MS} prescription. After renormalization the diagrams still contain mass singularities and infrared divergences. These are also controlled by dimensional regularization. Processes containing four partons in the final state masquerade as three jet events in the region in which one of the partons is soft and/or collinear with respect to another. The singularities present in this region are controlled by generalizing four particle phase space to n dimensions.

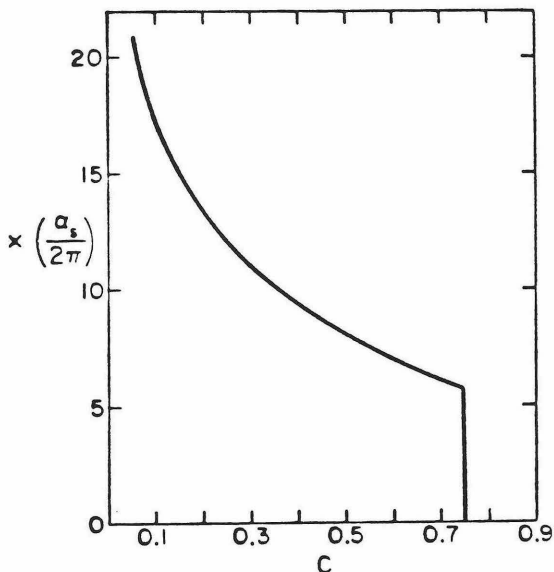


Fig. 1. $\frac{C}{\sigma_0} \frac{d\sigma}{dC}$ to $O(\alpha_s)$

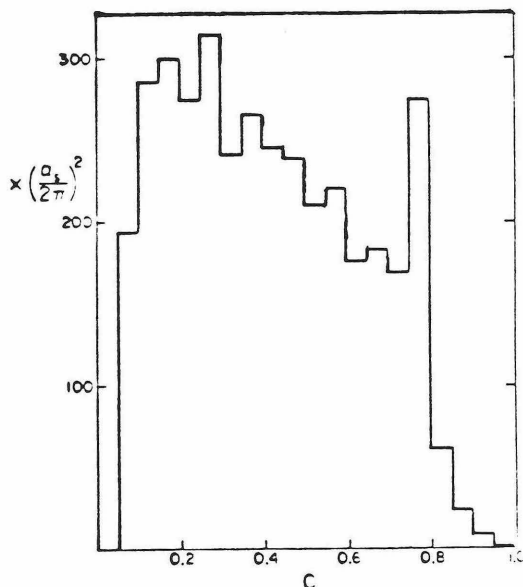


Fig. 2. $\frac{C}{\sigma_0} \frac{d\sigma}{dC}$ to $O(\alpha_s^2)$

In Fig. 2 we present our results for the $O(\alpha_s^2)$ contributions to $\frac{C}{\sigma_0} \frac{d\sigma}{dC}$ in units of $(\frac{\alpha_s}{2\pi})^2$ (the number of flavors is taken to be 5). An idea of the order of magnitude of the corrections with respect to the lower order term, Fig. 1, can be obtained by noting that for $Q = 30$ Gev, $\frac{\alpha_s(Q^2)}{2\pi} \sim \frac{1}{30}$ ($\Lambda = 500$ Mev); it is evident that they are compar-

able in size. Specifically, we may refer to all values of C greater than 0.5 as multijet events. Then, as an estimate of the size of the multijet fraction, we find

$$\int_{1/2}^1 \frac{1}{\sigma} \frac{d\sigma}{dC} dC = 2.8 \frac{\alpha_s(Q^2)}{2\pi} \left(1 + 37 \frac{\alpha_s(Q^2)}{2\pi} \right)$$

At $Q^2 \approx 30 \text{ GeV}$, the correction is 100%.

Some contributions to the cross section may be summed to all orders. The small C behavior has been shown to be

$$\frac{d\sigma}{dC} \sim \frac{\partial}{\partial C} \exp \left(-C_F \ln^2 \left(\frac{C}{2} \right) \frac{\alpha_s}{\pi} \right)$$

Furthermore, the continuation of Q^2 to positive values in the $\ln^2(-Q^2)$

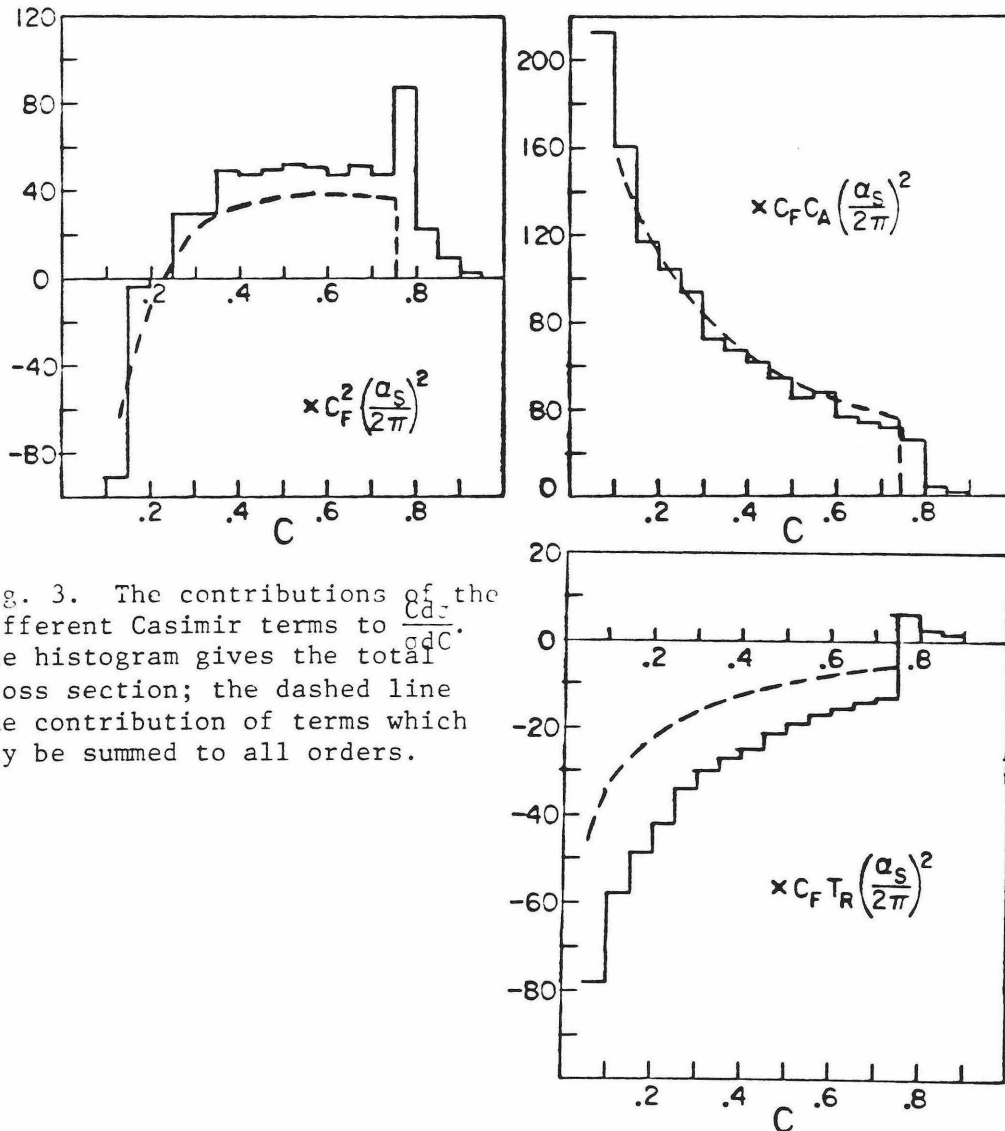


Fig. 3. The contributions of the different Casimir terms to $\frac{d\sigma}{dC}$. The histogram gives the total cross section; the dashed line the contribution of terms which may be summed to all orders.

terms from the loop integrations in the three parton final state diagrams gives rise to terms proportional to π^2 which, being associated with the leading poles, also may be exponentiated. Finally, the characteristic momentum of the interactions will be somewhat smaller than Q^2 . The presence of the term

$$\beta_0 \ln\left(\frac{s_{13}s_{23}}{Q^2}\right) \sim \beta_0 \ln\left(\frac{C}{6}\right)$$

where s_{ij} is the invariant mass of partons i and j and β_0 is the coefficient of g^3 in the expansion of the beta function, suggests that the running coupling constant should be evaluated at $QC/6$ rather than at Q . In Fig. 3 we have compared the sum of these terms with the $O(\alpha_s^2)$ contribution to the cross section. The terms proportional to C_F^2 , $C_F C_A$, and $C_F T_R$ are plotted separately. The dashed lines give

$$\text{L.O.} \left(-2C_F \ln^2\left(\frac{C}{2}\right) + \left(C_F + \frac{C_A}{2}\right)\pi^2 - \left(\frac{11C_A}{6} - \frac{2}{3} T_R\right) \ln\left(\frac{C}{6}\right) \right) \frac{\alpha_s}{2\pi}$$

where L.O. is the lowest order cross section. The histogram gives the total cross section. As can be seen, the remaining $O(\alpha_s^2)$ corrections are small.

1) R. K. Ellis, D. A. Ross, and A. E. Terrano, Caltech preprint CALT 68-785 (to be published in Nucl. Phys. B)

3. Perturbative Evaluation of Event Shapes in e^+e^- Annihilation

The observation in e^+e^- annihilation of planar hadronic events¹⁾ whose three jet structure can be interpreted as the result of gluon bremsstrahlung from a quark antiquark pair, directly reveals the constituent structure of the QCD field theory. The departure of the observed final hadronic state from a simple two jet configuration is proportional to the coupling of gluons to quarks in QCD perturbation theory and therefore is a sensitive measure of the strong coupling constant α_s . In this paper we calculate the first radiative correction ($O(\alpha_s^2)$) to the three jet structure necessary for the meaningful determination of $\alpha_s(Q^2)$ or equivalently the scale parameter of the strong interactions Λ .

Since the original proposal²⁾ that event shapes in e^+e^- annihilation would provide evidence for gluons, many variables^{3,4)} have been suggested to describe the jet structure of the final state hadrons. A theoretically acceptable variable must be insensitive to the emission of soft and/or collinear radiation. Variables, which combine parallel momenta linearly, are free from mass singularities and infrared divergences and hence are reliably calculable in a perturbation series⁵⁾ in $\alpha_s(Q^2)$.

The analysis we present calculates the shape of an e^+e^- hadronic event due to the production of massless quarks and gluons, instead of in terms of the observed particles which are hadrons and leptons with finite mass. Thus a further requirement to impose on jet variables is that they should be insensitive to the process of hadronization. At asymptotic energies this is certainly true since the effects of hadronization fall like powers of the center of mass energy Q relative to the leading terms. At presently investigated values of Q , understanding of the non-perturbative effects associated with hadronization is crucial to the extraction of information about the strong coupling constant. The interpretation of the experimental data also requires the inclusion of corrections due to the finite angular and energy acceptances of the particle

detection equipment. Moreover the shape of the final state is influenced by the proximity of heavy quark thresholds and the decay of resonant states (e.g., $\rho, J/\psi, T$). None of the above effects are included in our present analysis.

Nevertheless the calculation of the effects of perturbative QCD is a prerequisite for a complete analysis of event shapes in $e^+e^- \rightarrow$ hadrons. It is therefore this question which we address here.

We present our results in terms of global event shape parameters which do not require the determination of a jet axis. This gives a characterization of the event shape in terms of a continuous range of the parameter; no statement need be made about which jet a given hadron belongs to. Furthermore no minimization program (which for a large event multiplicity can be very costly in computer time) is required. Our results are presented in detail to allow the reader to extend them to include the effects which we have neglected.

We consider first of all the 3×3 tensor^{6,7)},

$$\theta^{ij} = \frac{\sum_a \frac{p_a^i p_a^j}{|p_a|}}{\sum_a |p_a|} \quad (1.1)$$

where the sum on a runs over all final state hadrons and p_a^i is the center of mass three-momentum of the a^{th} hadron^(F1). By principal axes transformation we can reduce θ to a diagonal tensor, the eigenvalues of which are given by the roots of the characteristic equation^(F2),

$$\lambda^3 - \lambda^2 + \frac{C}{3} \lambda - \frac{D}{27} = 0 \quad . \quad (1.2)$$

where we have used the condition that θ is normalized to have unit trace. In terms of the eigenvalues of θ , C and D are given by

$$D = 27 \lambda_1 \lambda_2 \lambda_3 \quad C = 3(\lambda_1 \lambda_2 + \lambda_2 \lambda_3 + \lambda_3 \lambda_1) \quad . \quad (1.3)$$

For a two-jet event both C and D vanish, whilst for a planar event,

$$C = 3\lambda_1(1 - \lambda_1) \quad , \quad (1.4)$$

and D vanishes. Hence the distribution in the variable C provides an effective measure of the multijet jet structure of the event with special emphasis on planar events. The distribution in D measures the deviation from planarity of the events. In Fig. 1 we display the contours of constant C and constant D on the eigenvalue plot. By imposing $C > 1/2$ we effectively exclude the two-jet region.

An alternative way to measure the structure of events is with the shape parameters⁴⁾,

$$H_\ell = \frac{4\pi}{(2\ell + 1)} \sum_{m=-\ell}^{m=\ell} \left| \sum_a Y_\ell^m(\Omega_a) \frac{|P_a|}{Q} \right|^2 \quad . \quad (1.5)$$

In eq. (1.5) the variable a is summed over all final state hadrons and P_a is the center of mass three momentum of the ath hadron and Ω_a the angle between its direction of motion and an arbitrary fixed axis. The first non-trivial shape parameter is H_2 which may also be written,

$$H_2 = \sum_{a,b} \frac{|P_a| |P_b|}{Q^2} P_2(\cos\theta_{ab}) \quad , \quad (1.6)$$

where P_2 is the second Legendre polynomial. Eq. (1.5) does not distinguish between events differing by the emission of soft and/or collinear particles and hence will be free of divergences in perturbation theory.

By expansion of the tensor θ^{ij} in spherical tensors we may easily show that two of the measures of event structure we have discussed are identical,

$$C \equiv (1 - H_2) \quad . \quad (1.7)$$

This identity is extremely useful. The quantity C is easier to visualize

because it is related to the reduction to principal axes of a momentum ellipsoid; on the other hand, eq. (1.6) for H_2 is a more convenient starting point for perturbative calculations since it is more readily cast into covariant form.

We now turn to the evaluation of the distribution of C or $(1 - H_2)$ in the perturbation theory of quarks and gluons. We consider the reactions,

$$e^+ e^- \rightarrow \gamma^*(Q) \rightarrow q\bar{q}, q\bar{q}G, q\bar{q}GG, q\bar{q}q\bar{q} \quad , \quad (1.8)$$

and we denote the final state parton momenta by p_i , where,

$$s_{ij} = (p_i + p_j)^2, \quad s_{ijk} = (p_i + p_j + p_k)^2, \quad y_{ij} = s_{ij}/Q^2, \quad (i < j < k), \quad (1.9)$$

and since we take the masses of partons to be zero, $p_i^2 = 0$.

In analogy with eq. (1.1) we construct a tensor from the parton variables of the final state,

$$\bar{\theta}^{ij} = \sum_{\text{partons } a} \frac{p_a^i p_a^j}{|p_a|} / \sum_{\text{partons } a} |p_a| \quad . \quad (1.10)$$

The tensor $\bar{\theta}$ which we calculate perturbatively differs only from the tensor θ by terms which vanish as an inverse power of the total center of mass energy,

$$\theta^{ij} = \bar{\theta}^{ij} + O(1/Q) \quad . \quad (1.11)$$

In complete analogy with the preceding discussion we can define the variables C and D for the tensor $\bar{\theta}$. The C parameters are given (for two, three and four particle final states respectively) by,

$$C^{(2)} = 0 \quad , \quad (1.12)$$

$$C^{(3)} = 3 \left[1 - \sum_{\substack{i,j=1 \\ i < j}}^3 \frac{s_{ij}^2}{(2p_i \cdot Q)(2p_j \cdot Q)} \right] \quad ,$$

$$= \frac{6 s_{12} s_{13} s_{23}}{(s_{12} + s_{13})(s_{12} + s_{23})(s_{13} + s_{23})} \quad . \quad (1.13)$$

$$C^{(4)} = 3 \left\{ 1 - \sum_{\substack{i,j=1 \\ i < j}}^4 \frac{s_{ij}^2}{(2p_i \cdot Q)(2p_j \cdot Q)} \right\} . \quad (1.14)$$

As a confirmation of our assertion that C is infrared finite, we may explicitly demonstrate that $C^{(4)}$ assumes the same form as $C^{(3)}$ in the region of collinear or soft emission by taking the appropriate limit. In the limit in which, for example, particles three and four become collinear eq. (1.14) becomes,

$$C^{(4)} \rightarrow \frac{6 s_{134} s_{234} (Q^2 - s_{134} - s_{234})}{(Q^2 - s_{134})(Q^2 - s_{234})(s_{134} + s_{234})} , \quad \begin{array}{l} s_{34} = 0 \\ s_{134}, s_{234} \text{ fixed} \end{array} . \quad (1.15)$$

Making the identification $s_{134} = s_{13}$ and $s_{234} = s_{23}$, eq. (1.15) reduces to eq. (1.13). The covariant expression for the variable D is given for a four parton final state by,

$$D^{(4)} = 27 \left[\frac{2(s_{12}s_{13}s_{24}s_{34} + s_{12}s_{14}s_{23}s_{34} + s_{13}s_{14}s_{23}s_{24}) - (s_{12}^2s_{34}^2 + s_{13}^2s_{24}^2 + s_{14}^2s_{23}^2)}{(s_{12} + s_{13} + s_{14})(s_{12} + s_{23} + s_{24})(s_{13} + s_{23} + s_{34})(s_{14} + s_{24} + s_{34})} \right] . \quad (1.16)$$

The structure of this paper is as follows. In the next section we calculate the differential cross section for processes involving three particles in the final state. Representing this as $\sigma^{(3)}$ we obtain the distribution in C,

$$\frac{d\sigma^{(3)}}{dC} = \int d\sigma^{(3)} \delta(C - C^{(3)}) , \quad (1.17)$$

where $C^{(3)}$ is the expression given by eq. (1.13). The above expression contains divergences due to the emission of soft and collinear particles. In Section III we calculate the contribution to the cross-section due to the production of four partons in the final state. This may be schematically written as,

$$\frac{d\sigma^{(4)}}{dC} = \int d\sigma^{(4)} \delta(C - C^{(4)}) , \quad (1.18)$$

where $C^{(4)}$ is given by eq. (1.14). Eq. (1.8) also contains singularities in the three-jet region. Thus the total contribution is given by,

$$\begin{aligned} \frac{d\sigma}{dC} &= \frac{d\sigma^{(4)}}{dC} + \frac{d\sigma^{(3)}}{dC} && C \neq 0 \\ &= d\sigma^{(4)} \delta(C - C^{(4)}) + d\sigma^{(3)} \delta(C - C^{(3)}) \end{aligned} \quad (1.19)$$

As a calculational device it is convenient to deal only with finite quantities. Hence we evaluate the terms in $d\sigma^{(4)}$ which contain singularities in the region in which four jets masquerade as three,

$$d\sigma^{(4)} \xrightarrow{\text{singular region}} d\sigma^{(s)} \quad (1.20)$$

We thus rewrite eq. (1.19).

$$\frac{d\sigma}{dC} = \left[d\sigma^{(4)} \delta(C - C^{(4)}) - d\sigma^{(s)} \delta(C - C^{(3)}) \right] + \left[(d\sigma^{(s)} + d\sigma^{(3)}) \delta(C - C^{(3)}) \right] \quad (1.21)$$

Each of the terms in square brackets is now finite in the three-jet region, (but still contains divergences in the two-jet region ($C=0$)); the first is finite by construction and the second by virtue of KLN theorem⁹). The calculation of $\frac{d\sigma}{dD}$ is much less complex because for $D \neq 0$ it receives contributions from $d\sigma^{(4)}$ alone. In Section IV we present our numerical results for the above distributions. Our conclusions are presented in Section V.

II. Processes involving two and three particles in the final state

As explained in the previous section our operating procedure is to calculate the contributions to the event shape of the various processes^(F3).

$$e^+e^- \rightarrow q(p_1) + \bar{q}(p_2) \quad ; \quad (2.1)$$

$$e^+e^- \rightarrow q(p_1) + \bar{q}(p_2) + G(p_3) \quad ; \quad (2.2)$$

$$e^+e^- \rightarrow q(p_1) + \bar{q}(p_2) + G(p_3) + G(p_4) \quad ; \quad (2.3)$$

$$e^+e^- \rightarrow \bar{q}(p_1) + \bar{q}(p_2) + q(p_3) + q(p_4) \quad , \quad (2.4)$$

where the symbols in brackets denote the momenta which we assign to the various particles. In this section we present our results for eq. (2.2). Our treatment of the processes with four particles in the final state is given in Section III.

There exists a certain region of phase space, corresponding to the soft or collinear emission of a gluon in which the three-jet process shown in Fig. 2b,c, simulates a two-jet event shown in Fig. 2a. This is precisely the region in which the intermediary propagators vanish and individual transition probabilities contain divergences, which vanish in the total transition probability after the inclusion of virtual gluon exchange as a consequence of the KLN theorem⁹⁾.

We choose to regulate these divergences, as well as the normal ultraviolet divergences by continuing the dimensionality¹¹⁾ of spacetime n to $n = (4-2\varepsilon)$. In this scheme the phase space for the massless final state particles is modified so that,

$$(PS)^{(j)} = (2\pi)^n \int \left(\prod_{i=1}^j \frac{d^n p_i}{(2\pi)^{n-1}} \delta^+(p_i^2) \right) \delta^n(Q - \sum_{i=1}^j p_i) \quad (2.5)$$

After performing angular integrations we obtain

$$(PS)^{(2)} = A_0 \int ds_{12} \delta(y_{12} - 1) \frac{1}{4Q^4} \quad (2.6)$$

$$(PS)^{(3)} = \frac{A_0}{8} \left(\frac{1}{8\pi^2} \left(\frac{4\pi}{Q^2} \right)^\epsilon \frac{1}{\Gamma(1-\epsilon)} \right) \int dy_{13} dy_{23} (y_{13} y_{23} (1-y_{13}-y_{23}))^{-\epsilon} \theta(1-y_{13}-y_{23}) \quad (2.7)$$

$$\text{where } A_0 = \left(\frac{1}{2\pi} \frac{\Gamma(1-\epsilon)}{\Gamma(2-2\epsilon)} \left(\frac{4\pi}{Q^2} \right)^\epsilon Q^2 \right) .$$

The matrix elements are calculated as follows. The first step is to calculate the transition probability for a virtual photon of mass Q^2 to produce the various final states eqs. (2.1-2.4). If we integrate over the angular correlations between the final state and the incoming beams the summation over the polarizations of the incoming virtual photon may be replaced by $-g^{\mu\nu}$

$$\sum_{\text{polarization}} \epsilon^\mu(Q) \epsilon^{\nu*}(Q) = -g^{\mu\nu} \quad (2.8)$$

Explicit calculations of this matrix element and all other matrix elements in this paper are calculated in n dimensions using GAMALG¹²⁾ which is implemented in MACSYMA¹³⁾. The result for the two-jet cross section, which defines our normalization is given by,

$$\frac{1}{\sigma_0} d\sigma^{(2)} = H \int dy_{12} \delta(y_{12} - 1) ; \quad H = 1 + O(\epsilon) \quad , \quad (2.9)$$

where $\sigma_0 = \frac{4\pi\alpha^2}{3Q^2} N_C \sum_{k=1}^{n_f} e_k^2$ and $N_C = 3$ is the number of colors, n_f is the number of flavors, e_k is the charge of the quark in units of the proton charge and H is a constant of proportionality equal to one in four dimensions.

From the three-jet diagrams of Fig. 2 we obtain,

$$\frac{1}{\sigma_0} \frac{d\sigma^{(3)}}{ds_{13} ds_{23}} = H \frac{\alpha_s}{2\pi} C_F \left(\frac{4\pi\mu^2}{Q^2} \right)^\epsilon \frac{1}{\Gamma(1-\epsilon)} \frac{1}{Q^4} T(s_{12}, s_{13}, s_{23}) \theta(1-y_{13}-y_{23}) (y_{13} y_{23} (1-y_{13}-y_{23}))^{-\epsilon} \quad (2.10)$$

where

$$T(s_{12}, s_{13}, s_{23}) = \left\{ \frac{(1-\epsilon)s_{23}}{s_{13}} + \frac{(1-\epsilon)s_{13}}{s_{23}} + \frac{2[s_{12}(s_{12} + s_{13} + s_{23}) - \epsilon s_{13}s_{23}]}{s_{13}s_{23}} \right\}, \quad (2.11)$$

and μ is an arbitrary parameter with the dimensions of mass included to keep the coupling constant dimensionless in n dimensions. From eq. (2.10) alone we can calculate $\frac{1}{\sigma_0} \frac{d\sigma^{(3)}}{dC}$ for all values of C except in the two-jet region ($C=0$) where there are infrared divergences. Setting $\epsilon = 0$ and introducing the more usual variables $x_1 = 1-y_{23}$, $x_2 = 1-y_{13}$, we have,

$$\frac{1}{\sigma_0} \frac{d\sigma}{dC} = \frac{\alpha_s}{2\pi} C_F \int_0^1 dx_1 \int_0^1 dx_2 \theta(x_1+x_2-1) \frac{x_1^2+x_2^2}{(1-x_1)(1-x_2)} \delta\left(C - \frac{6(1-x_1)(1-x_2)(x_1+x_2-1)}{x_1x_2(2-x_1-x_2)}\right) \quad (2.12)$$

Performing the delta function integration we obtain

$$\frac{1}{\sigma_0} \frac{d\sigma^{(3)}}{dC} = \frac{\alpha_s}{2\pi} C_F \int_{x_2^-(C)}^{x_2^+(C)} dx \frac{6x[C(x^3 + (x-2)^2) - 6(1-x)(1+x^2)]}{C(C+6)^2(x - \frac{6}{C+6}) \sqrt{(\frac{6}{C+6} - x)(x_2^+ - x)(x - x_2^-)x}} \quad (2.13)$$

where

$$x_2^\pm(C) = \frac{1 + \frac{2C}{3} \pm \sqrt{(1 - \frac{4C}{3})}}{(\frac{C}{3} + 2)} \quad (2.14)$$

From the above integral we can obtain the limiting asymptotic form around the three-jet value $C = 3/4$,

$$\frac{C}{\sigma_0} \frac{d\sigma^{(3)}}{dC} \Big|_{C=\frac{3}{4}} = C_F \left(\frac{2^6 \pi}{3^3 \sqrt{3}} \right) \frac{\alpha_s}{2\pi} = (5.73) \frac{\alpha_s}{2\pi} \quad (2.15)$$

A plot⁴⁾ of $\frac{1}{\sigma} \frac{d\sigma^{(3)}}{dC}$ is shown in Fig. 3. This plot together with the information on the value of the total cross section through order (α_s) completely specifies the distribution. The whole C distribution can be computed by adding

a delta function at the origin whose coefficient is such that the area under the curve is equal to the known perturbatively corrected total cross-section. Employing the $\overline{\text{MS}}$ subtraction scheme¹⁴⁾, this result for this quantity is given by^{15,16)},

$$\begin{aligned} \frac{1}{\sigma_0} \sigma &= 1 + \frac{\alpha_s(Q^2)}{2\pi} \left(\frac{3}{2} C_F \right) + \left(\frac{\alpha_s(Q^2)}{2\pi} \right)^2 \left[C_F \left(\frac{123 N_C}{8} - \frac{3}{8} C_F - \frac{11}{2} T_R - 6 \zeta(3) b_0 \right) \right] \\ &\equiv 1 + \frac{\alpha_s(Q^2)}{\pi} + \left(\frac{\alpha_s(Q^2)}{\pi} \right)^2 (1.986 - 0.115 n_f) \quad , \end{aligned} \quad (2.16)$$

where¹⁷⁾,

$$\begin{aligned} \frac{\alpha_s(Q)^2}{2\pi} &= \frac{1}{[b_0 \ell \pi Q^2 / \Lambda^2 + b_1 / b_0 \ell \pi (\ell \pi Q^2 / \Lambda^2)]} \\ \xi(3) &= 1.2021, \quad b_0 = \frac{11 N_C - 4 T_R}{6}, \quad b_1 = \left(\frac{17}{6} N_C^2 - \frac{5}{3} N_C T_R - C_F T_R \right) \quad , \end{aligned} \quad (2.17)$$

and the Casimir operators are $C_F = \frac{4}{3}, N_C = 3, T_R = \frac{n_f}{2}$. At present we are interested only in the $O(\alpha_s)$ correction but we include the $O(\alpha_s^2)$ correction for later convenience.

The radiative corrections to the three gluon cross-section are shown in Fig. 4. In order α_s^2 they give contributions because of their interference with the lower order diagrams of Fig. 2b,c. To calculate the corrections we found it most efficient to square the amplitudes and perform the traces to reduce the transition probability to a Lorentz scalar, before integrating over the virtual gluon loop momentum ℓ .

It is then convenient to shift numerator factors so that they cancel against denominators. For example, we rewrite,

$$\frac{\ell \cdot p_2}{\ell^2 (\ell - p_2)^2 (\ell + p_3)^2 (\ell + p_1 + p_3)^2} \rightarrow \frac{1}{2(\ell - p_2)^2 (\ell + p_3)^2 (\ell + p_1 + p_3)^2} - \frac{1}{2\ell^2 (\ell + p_3)^2 (\ell + p_1 + p_3)^2} \quad . \quad (2.18)$$

By so doing we reduce the problem to a set of standard integrals involving fewer denominators and fewer powers of the loop momentum in the numerator. To aid the reader who wishes to check our results we have presented our results for certain integrals in Appendix A.

We perform calculations in the Feynman gauge. As previously noted the ultraviolet divergences are controlled by dimensional regularization. We perform renormalization in the so-called $\overline{\text{MS}}$ scheme which corresponds to the subtraction of ultraviolet poles together with the attendant Euler-Mascheroni constant and $\ell_n 4\pi$. The $\overline{\text{MS}}$ counterterm is given by,

$$\frac{1}{\sigma_0} d\sigma^{\text{CT}} = H \left(\frac{\alpha_s}{2\pi} \right) C_F \left(\frac{4\pi\mu^2}{Q^2} \right)^\epsilon \frac{1}{\Gamma(1-\epsilon)} \frac{1}{Q^4} \int ds_{13} ds_{23} T(Q^2 - s_{13} - s_{23}, s_{13}, s_{23}) (y_{13} y_{23} (1 - y_{13} - y_{23}))^{-\epsilon}$$

$$\left[\left(\frac{\alpha_s}{2\pi} \right) \frac{\Gamma(1-\epsilon)}{\Gamma(1-2\epsilon)} \left(\frac{4\pi\mu^2}{Q^2} \right)^\epsilon \left(\frac{2T_R}{3} - \frac{11N_C}{6} \right) \left(\frac{1}{\epsilon} + \ell_n Q^2/\mu^2 \right) + 0(\epsilon) \right], \quad (2.19)$$

up to terms of order ϵ and higher which have been added so that eq. (2.19) can be cast in a convenient form. The function T, defined in eq. (2.11) gives the kinematic structure of the $O(\alpha_s)$ cross section.

In intermediate stages of the calculation the length of the expression becomes large, but the final result for the three-gluon cross-section assumes the relatively simple form

$$\frac{1}{\sigma_0} d\sigma^{(3)} = H \frac{\alpha_s(Q^2)}{2\pi} C_F \left(\frac{4\pi\mu^2}{Q^2} \right)^\epsilon \frac{1}{\Gamma(1-\epsilon)Q^4} \int ds_{12} ds_{13} ds_{23} (y_{12} y_{13} y_{23})^{-\epsilon} \delta(Q^2 - s_{12} - s_{13} - s_{23})$$

$$\times \left\{ T(s_{12}, s_{13}, s_{23}) \left[1 + \frac{\alpha_s}{2\pi} \frac{\Gamma(1-\epsilon)}{\Gamma(1-2\epsilon)} \left(\frac{4\pi\mu^2}{Q^2} \right)^\epsilon \right. \right.$$

$$\left. \left. \times \left(\frac{2C_F + N_C}{-\epsilon^2} - \frac{1}{\epsilon} \left(3C_F - 2C_F \ell_n y_{12} + \frac{11}{6} N_C + N_C \ell_n \frac{y_{12}}{y_{13} y_{23}} - \frac{2}{3} T_R \right) \right) \right] + \frac{\alpha_s}{2\pi} F(s_{12}, s_{13}, s_{23}) \right.$$

$$\left. \left. + \frac{\alpha_s}{2\pi} \left[T(s_{12}, s_{13}, s_{23}) \left(\frac{2\pi^2}{3} (C_F + \frac{N_C}{2}) - 8C_F - C_F \ell_n^2 y_{12} + \frac{N_C}{2} (\ell_n^2 y_{12} - \ell_n^2 y_{13} - \ell_n^2 y_{23}) \right) \right] \right\}, \quad (2.20)$$

where the function F is defined as

$$\begin{aligned}
 F(s_{12}, s_{13}, s_{23}) = & \left\{ C_F \left[\frac{s_{12}}{s_{12} + s_{13}} + \frac{s_{12}}{s_{12} + s_{23}} + \frac{s_{12} + s_{23}}{s_{13}} + \frac{s_{12} + s_{13}}{s_{23}} \right] \right. \\
 & + \ell\pi y_{13} \left[\frac{C_F (4s_{12}^2 + 2s_{12}s_{13} + 4s_{12}s_{23} + s_{13}s_{23})}{(s_{12} + s_{23})^2} + \frac{N_C s_{13}}{(s_{12} + s_{23})} \right] \\
 & + \ell\pi y_{23} \left[\frac{C_F (4s_{12}^2 + 2s_{12}s_{23} + 4s_{12}s_{13} + s_{13}s_{23})}{(s_{12} + s_{13})^2} + \frac{N_C s_{23}}{(s_{12} + s_{13})} \right] \\
 & - 2 \left(C_F - \frac{N_C}{2} \right) \left[\frac{s_{12}^2 + (s_{12} + s_{13})^2}{(s_{13}s_{23})} R(y_{12}, y_{23}) + \frac{s_{12}^2 + (s_{12} + s_{23})^2}{s_{13}s_{23}} R(y_{12}, y_{13}) + \frac{Q^2 (s_{13}^2 + s_{23}^2)}{s_{13}s_{23}(s_{13} + s_{23})} \right. \\
 & \left. - 2 \ell\pi y_{12} \left(\frac{s_{12}^2}{(s_{13} + s_{23})^2} + \frac{2s_{12}}{(s_{13} + s_{23})} \right) - N_C T(s_{12}, s_{13}, s_{23}) R(y_{13}, y_{23}) \right] . \quad (2.21)
 \end{aligned}$$

and the function R is defined as,

$$R(x, y) = \left[\ell\pi x \ell\pi y - \ell\pi x \ell\pi (1-x) - \ell\pi y \ell\pi (1-y) + \frac{\pi^2}{6} - \text{Li}_2(x) - \text{Li}_2(y) \right] , \quad (2.22)$$

where $\text{Li}_2(x)$ is the normal dilogarithm function

$$\text{Li}_2(x) = - \int_0^x \frac{\ell\pi (1-z)}{z} dz . \quad (2.23)$$

Several features of eq. (2.20) are worthy of note. Firstly, the coupling constant in eq. (2.20) is now the running coupling constant defined in the $\overline{\text{MS}}$ scheme. Secondly, the divergent terms coming from the emission of soft and collinear radiation have the same form as the lowest order cross-section (modulo logarithms). Thirdly, we note the appearance of π^2 terms proportional to the lowest order cross section which are intimately related to the soft singularity

$$\text{Re} \left\{ \left(\frac{4\pi\mu^2}{-Q^2} \right)^\epsilon \left(-\frac{2}{\epsilon} \right) \right\} = \left(\frac{4\pi\mu^2}{Q^2} \right)^\epsilon \left(-\frac{2}{\epsilon} + \pi^2 \right) \left(\frac{4\pi\mu^2}{Q^2} \right)^\epsilon + O(\epsilon) \quad . \quad (2.24)$$

This concludes our discussion of the three-parton final state.

III. Calculation of Diagrams Involving Four Particles in the Final State

The aim of this section is to present the calculation of diagrams with four partons in the final state, set up in such a way that the singularities which occur when a four jet event masquerades as a three jet event (i.e., the region of one soft and/or collinear emission) can be easily extracted. Since we are interested in calculating a Lorentz invariant quantity, we are at liberty to evaluate different terms in the transition probability in different Lorentz frames.

For example, if we are interested in a term which contains the denominator s_{13} , it is convenient to set up the four body phase space as a "quasi three body production"

$$\begin{array}{l}
 Q \rightarrow p_{13} + p_2 + p_4 \\
 \quad \quad \quad \downarrow \\
 \quad \quad \quad \quad \rightarrow (p_1 + p_3)
 \end{array} \quad . \quad (3.1)$$

We shall refer to this as the "1-3 system." To write down the four-particle phase space in this system we move to the center of mass frame of the produced composite,

$$p_1 = \frac{\sqrt{s_{13}}}{2} (1, \dots, \sin\theta\cos\theta', \cos\theta) \quad (3.2)$$

$$p_3 = \frac{\sqrt{s_{13}}}{2} (1, \dots, -\sin\theta\cos\theta', -\cos\theta) \quad (3.3)$$

$$p_2 = \frac{s_{123} - s_{13}}{2\sqrt{s_{13}}} (1, \dots, 0, 1) \quad (3.4)$$

$$p_4 = \frac{s_{134} - s_{13}}{2\sqrt{s_{13}}} (1, \dots, \sin\beta, \cos\beta) \quad (3.5)$$

where the dots in eqs. (3.2, 3.3) indicate $n - 3$ unspecified, equal and opposite angles (in n dimensions) and $n - 3$ zeros in eqs. (3.4, 3.5). Four

momentum conservation constrains $\cos\theta$,

$$\frac{(1-\cos\theta)}{2} = \frac{s_{13}(Q^2 - s_{123} - s_{134} + s_{13})}{(s_{123} - s_{13})(s_{134} - s_{13})} \quad . \quad (3.6)$$

Setting $v = \frac{1-\cos\theta}{2}$, we obtain for the n dimensional phase space in this system,

$$\begin{aligned} (\text{PS})^{(4)} = A_0 \{ & \left(\frac{1}{8\pi^2}\right) \left(\frac{4\pi}{Q^2}\right)^\epsilon \frac{1}{\Gamma(1-\epsilon)} \left(\frac{S Q^2}{16}\right) \int dy_{123} dy_{134} dy_{13} (y_{123} y_{134} - y_{13})^{-\epsilon} \\ & (y_{13}^{+1} - y_{123} - y_{134})^{-\epsilon} (y_{13})^{-\epsilon} \theta(y_{13}) \theta(y_{123} y_{134} - y_{13}) \theta(y_{13}^{+1} - y_{123} - y_{134}) \\ & \int_0^1 dv (v(1-v))^{-\epsilon} \frac{1}{N_{\theta'}} \int_0^\pi d\theta' \sin^{-2\epsilon} \theta' \} \quad . \quad (3.7) \end{aligned}$$

A_0 is given in eq. (2.7), S is the statistical factor and $N_{\theta'}$ is a normalization factor determined such that

$$\int_0^\pi d\theta' \sin^{-2\epsilon} \theta' = N_{\theta'} = 2^{2\epsilon} \pi \frac{\Gamma(1-2\epsilon)}{\Gamma^2(1-\epsilon)} \quad . \quad (3.8)$$

After integration over θ' and v , the angular distribution of the produced composite s_{13} , the form of the phase space distribution is very similar to the three particle phase space (eq. (2.7)), except for the differing range of integration. The lower limit of the y_{13} integration is specified by the θ functions,

$$\theta(y_{13}) \theta(y_{13}^{+1} - y_{123} - y_{134}) \rightarrow \theta(y_{13}) \theta(1 - y_{123} - y_{134}) + \theta(y_{123} + y_{134} - 1) \theta(y_{13}^{+1} - y_{123} - y_{134})$$

so the range of the s_{13} integration is split so that,

$$\int dy_{13} \rightarrow \theta(1 - y_{123} - y_{134}) \int_0^{y_{123} y_{134}} dy_{13} + \theta(y_{123} + y_{134} - 1) \int_{y_{123} + y_{134} - 1}^{y_{123} y_{134}} dy_{13} \quad .$$

A term containing a denominator s_{13} will give a singularity only in the first region of integration. The structure of this first region of integration when substituted into eq. (3.7) is exactly analogous to eq. (2.7). Possible

divergences resulting from the emission of parton 3 collinear and/or soft with respect to parton 1 are associated with the integrations over s_{13} , v and θ' in the first region of s_{13} integration.

The calculation of the transition probability for the process

$$\gamma^*(Q) \rightarrow q(p_1) + \bar{q}(p_2) + G(p_3) + G(p_4) \quad (3.9)$$

from the eight diagrams shown in Fig. (5) contains in principle 36 terms. Many of them are related by interchange of momentum labels and, in all, only 13 transition probabilities need be calculated. In Table (1) we give the momentum label interchanges necessary to generate all the transition probabilities from the thirteen which we choose to calculate. The interference of graph B_i with B_j is written as B_{ij} , ($i \geq j$).

It is therefore sufficient to consider the thirteen transition probabilities on the top row of Table (1), which we display in Fig. (6). The on-shell partons are denoted by the cutting lines and the numbers refer to the labels of the external legs. The transition probabilities are seen to fall into three classes:

- A) Planar QED type graphs with group weight C_F^2
- B) Non-planar QED type graphs with group weight $C_F(C_F - \frac{N_C}{2})$
- C) QCD graphs involving the three gluon vertex with group weight $C_F N_C$.

All matrix elements are generated in n dimensions using GAMALG. We sum over the two physical polarizations of the produced gluons. This is most easily accomplished by summing over the polarizations with

$$\sum_{\text{pol}} \epsilon^{\mu*} \epsilon^{\nu} = -g^{\mu\nu} \quad (3.10)$$

but including "ghost loop graphs" in diagrams B77, B87 (and B88) to take account of the fact that the gluon current is not conserved.

Our method of calculation of the event shape parameter C depends crucially on our ability to divide the transition probabilities into pieces which are divergent in the three jet region when a single denominator from the set s_{13} , s_{23} , s_{14} , s_{24} , or s_{34} vanishes. This is clearly always possible since the vanishing, for example, of s_{13} corresponds to the region in which gluon p_3 is collinear and/or soft with respect to quark p_1 . In the Feynman gauge (cf. eq. (3.10)), - and in all but physical gauges - a particular diagram contains overlapping infrared divergences. Individual graphs diverge as any one of several s_{ij} 's vanish, reflecting the fact that it may be made to simulate a three jet diagram in several different ways. We divide each graph into pieces which only contain singularities as a single s_{ij} vanishes. These various pieces correspond to the different ways that a four parton final state can assume three jet structure because of the coalescence of two partons.

Two examples will clarify our procedure. Suppressing numerator factors graph B52 (Fig. 6) may be written as

$$B52 \sim \frac{1}{s_{134}^2 s_{13} s_{14}} \quad . \quad (3.11)$$

The potentially dangerous terms in eq. (3.11) are s_{13} and s_{14} , since s_{134} can vanish only in the two jet configuration in which partons 1, 3 and 4 recoil against parton 2. Partial fractioning eq. (3.11), we get,

$$B52 \sim \frac{1}{s_{134}^2 s_{13} (s_{13} + s_{14})} + \frac{1}{s_{134}^2 s_{14} (s_{13} + s_{14})} \quad . \quad (3.12)$$

The first term in eq. (3.12) should be calculated in the "1-3 system" eq. (3.2 - 3.5). In this system s_{134} is one of the subsequent variables of integration and hence for the purposes of the s_{13} integration it is held fixed. Both denominators s_{13} and $(s_{13} + s_{14})$ may vanish (at fixed s_{134} and

s_{123}) but the latter only when s_{13} also vanishes, since s_{13} and s_{14} are both positive semi-definite

$$(s_{13}+s_{14}) \rightarrow 0 \quad (s_{13}=0, \cos\theta = 1) \quad . \quad (3.13)$$

The treatment of the second term in eq. (3.12) is identical in the "1-4 system".

Partial fractioning similar to the above must be applied throughout. For example, suppressing most of the numerator, graph B41 (Fig. 6) is given by,

$$B41 \sim \frac{s_{12}}{(s_{13}s_{14}s_{23}s_{24})} \quad . \quad (3.14)$$

Performing successive partial fractioning we rewrite this term as,

$$\frac{s_{12}}{s_{13}s_{14}s_{23}s_{24}} \equiv \left[\frac{s_{12}}{(s_{24}-s_{13})(s_{13}+s_{14})(s_{13}+s_{23})s_{13}} + (3\leftrightarrow 4) + (1\leftrightarrow 2) + (3\leftrightarrow 4, 1\leftrightarrow 2) \right]. \quad (3.15)$$

The first term in eq. (3.15) (written out explicitly) is singular as $s_{13} \rightarrow 0$.

In the "1-3 system" we may write its singular part,

$$\frac{s_{12}}{(s_{24}-s_{13})(s_{13}+s_{14})(s_{13}+s_{23})s_{13}} \xrightarrow{s_{13} \rightarrow 0} \frac{s_{123}}{(Q^2-s_{123}-s_{134})s_{134}(s_{13}^v+s_{123}(1-v))s_{13}} \quad \text{fixed } s_{123}, s_{134} \quad . \quad (3.16)$$

The right-hand side of eq. (3.16) contains two denominators singular in the three jet region but both require the vanishing of s_{13} . For this argument the presence of the s_{12} factor in the numerator is essential. In the "1-3 system" when s_{13} vanishes partons 2 and 4 are parallel so that s_{12} and s_{14} are proportional to one another. The constant of proportionality depends only on the variables s_{123} and s_{134} which are kept fixed during the s_{13} integration. Hence in the singular limit $s_{12}/(s_{13}+s_{14})$ is replaced by a

constant. The denominators s_{134} and $(Q^2 - s_{123} - s_{134})$ can also vanish but only in the two-jet region $C = 0$.

Our calculation procedure is as follows. We first calculate all the transition probabilities in n dimensions. The full result for $d\sigma^{(4)}$ in four dimensions is given in Appendix B. We then partial fraction, as described in the previous paragraph so that the resultant pieces are divergent in the three-jet region only when a single s_{ij} vanishes. We then collect together all the terms corresponding to the various s_{ij} . The answers fall into different pieces identified by differing group weight factors. Here in the text we present the singular parts of these terms in the three-jet region for spacetime dimensionality $n = 4 - 2\epsilon$. After integration the singularities of these pieces will explicitly cancel against the poles in the virtual diagrams (eq. (2.20)).

The part of the four-parton cross section which is singular when a quark and a gluon are collinear (or soft) with respect to one another is given by ^(F4)

$$\begin{aligned} \frac{1}{\sigma_0} d\sigma_I(s) &= H \frac{\alpha_s}{2\pi} C_F \left(\frac{4\pi\mu^2}{Q^2} \right)^\epsilon \frac{1}{\Gamma(1-\epsilon)} \frac{1}{Q^4} \left[\int ds_{123} ds_{134} ds_{13} (y_{123} y_{134})^{-\epsilon} (1-y_{123}-y_{134})^{-\epsilon} (y_{13})^{-\epsilon} \right. \\ &\theta(y_{13}) \theta(y_{123} y_{134} - y_{13}) \theta(1-y_{123}-y_{134}) \int_0^1 dv (v(1-v))^{-\epsilon} \frac{1}{N_\theta} \int_0^\pi d\theta' \sin^{-2\epsilon}\theta' \\ &\frac{1}{2} \frac{\alpha_s}{2\pi} \left(\frac{4\pi\mu^2}{Q^2} \right)^\epsilon \frac{1}{\Gamma(1-\epsilon)} \frac{T(s_{123}, s_{134}, Q^2 - s_{123} - s_{134})}{s_{13}} \\ &\left[C_F \left(\frac{2s_{123}}{(s_{13}v + s_{123}(1-v))} - 1 - v - \epsilon(1-v) \right) + N_C \left(\frac{s_{134}}{(s_{13}v + s_{134}(1-v))} - \frac{s_{123}}{(s_{13}v + s_{123}(1-v))} \right) \right] \\ &+ \left[\{3 \leftrightarrow 4\} + \{1 \leftrightarrow 2\} + \{1 \leftrightarrow 2, 3 \leftrightarrow 4\} \right] \end{aligned} \quad , \quad (3.17)$$

and the function T is given in eq. (2.11). The above formula is to be interpreted with v and θ' transforming under the indicated interchanges. Under (3 \leftrightarrow 4) interchange (i.e., transforming from the "1-3 system" to the "1-4 system") we have

$$v = \frac{s_{12}}{s_{12} + s_{23}} \rightarrow \tilde{v} = \frac{s_{12}}{s_{12} + s_{24}}$$

$$(1 - \sin\theta\cos\theta'\sin\beta - \cos\theta\cos\beta) = \frac{s_{14}}{s_{14} + s_{34}} \rightarrow \frac{s_{13}}{s_{13} + s_{34}} = (1 - \sin\tilde{\theta}\cos\tilde{\theta}'\sin\tilde{\beta} - \cos\tilde{\theta}\cos\tilde{\beta})$$

(3.18)

and similarly for the other interchanges. Several features of eq. (3.17) should be noted. Firstly it has the kinematic structure of the $O(\alpha_s)$ matrix element. It is proportional to the matrix element squared T in which particles one and three (or the other interchanges) are considered as a single composite. Also the coefficient of the s_{13} singularity proportional to C_F may be written for $v \neq 1$ as

$$P_{qq}^{n \neq 4}(v) = C_F \left(\frac{2}{1-v} - 1 - v - \varepsilon(1-v) \right),$$

which is seen to be the generalization to n dimensions of the Altarelli-Parisi function¹⁸⁾. The other singular contributions in eq. (3.17) are proportional to N_C . These are terms, which are singular in the three-jet region but make no contribution, in the leading log approximation. They are therefore not related to Altarelli-Parisi kernels. The existence of these terms indicates that the leading log approximation may not be used to extract information about subleading logs.

The other terms proportional to the N_C are singular in the limit when a pair of gluons become collinear and/or parallel. Their contribution is,

$$\begin{aligned}
 \frac{1}{\sigma_0} d\sigma_{II}(s) &= H \frac{\alpha_s}{2\pi} C_F \left(\frac{4\pi\mu^2}{Q^2} \right)^\epsilon \frac{1}{\Gamma(1-\epsilon)} \frac{1}{Q} \int ds_{134} ds_{234} ds_{34} (y_{134} y_{234})^{-\epsilon} (1-y_{134}-y_{234})^{-\epsilon} (y_{34})^{-\epsilon} \\
 &\theta(y_{34}) \theta(y_{134} y_{234} - y_{34}) \theta(1-y_{134}-y_{234}) \int_0^1 dv (v(1-v))^{-\epsilon} \frac{1}{N_{\theta'}} \int_0^\pi d\theta' \sin^{-2\epsilon}\theta' \\
 &\frac{1}{2} \frac{\alpha_s}{2\pi} \left(\frac{4\pi\mu^2}{Q^2} \right)^\epsilon \frac{1}{\Gamma(1-\epsilon)} \frac{N_C}{s_{34}} \left\{ T(Q^2 - s_{134} - s_{234}, s_{134}, s_{234}) \right. \\
 &\left[\frac{s_{234}}{(s_{34} + s_{23})} + \frac{s_{234}}{(s_{34} + s_{24})} + \frac{s_{134}}{(s_{34} + s_{13})} + \frac{s_{134}}{(s_{34} + s_{14})} \right. \\
 &\left. \left. - 4 + 2v(1-v) \right] + (2(1-\epsilon)\cos^2\theta' - 1) 4v(1-v) \frac{Q^2(Q^2 - s_{134} - s_{234})}{s_{134}s_{234}} \right\} . \quad (3.19)
 \end{aligned}$$

Here again the result has the kinematic structure of the lowest order with partons 3 and 4 interpreted as a single particle (plus terms which vanish after integration over θ'). In this formula θ' and v are the angles appropriate to the "3-4 system" ^(F7). To check our results we note that after integration over θ' for $v \neq 0,1$ we obtain the Altarelli-Parisi kernel ¹⁸⁾

$$P_{GG}(v) = N_C \left[\frac{2}{v} + \frac{2}{1-v} - 4 + 2v(1-v) \right] . \quad (3.20)$$

This kernel is unchanged in n dimensions.

Lastly we calculate the matrix elements for the process,

$$\gamma^*(Q) \rightarrow \bar{q}(p_1) + \bar{q}(p_2) + q(p_3) + q(p_4) , \quad (3.21)$$

from the diagrams shown in Fig. 7. Only twelve of the possible thirty-six transition probabilities are independent. In Table (2) we display the interchanges necessary to recover all the transition probabilities from the twelve which we choose to calculate. These twelve transition probabilities are shown

graphically in Fig. 8 where the cutting lines indicate the particles which are on-shell. The diagrams clearly fall into three classes distinguished by their group weight factors. Diagrams A81, A82 and A53 together with their companions generated by interchange (Class F) give no contribution in an experiment in which the charge of the final particles is not detected. This is a consequence of charge conjugation - the non-Abelian generalization of Furry's theorem¹⁹⁾. The matrix elements for the remaining two classes (D and E) are given in four dimensions in Appendix B. Here in the text we quote only the pieces singular in the three-jet region, in n dimensions,

$$\begin{aligned} \frac{1}{\sigma_0} d\sigma_{III}^{(s)} &= H \frac{\alpha_s}{2\pi} C_F \left(\frac{4\pi\mu^2}{Q^2}\right)^\epsilon \frac{1}{\Gamma(1-\epsilon)} \frac{1}{Q^4} \left\{ \int ds_{123} ds_{134} ds_{13} [(y_{123}y_{134})^{1-y_{123}-y_{134}} y_{13}]^{-\epsilon} \right. \\ &\quad \left. \theta(y_{13})^\epsilon (y_{123}y_{134}-y_{13})^\theta (1-y_{123}-y_{134}) \int_0^1 dv (v(1-v))^{-\epsilon} \frac{1}{N_{\theta'}} \int_0^\pi d\theta' \sin^{-2\epsilon}\theta' \right. \\ &\quad \left. \frac{1}{4} \frac{\alpha_s}{2\pi} \left(\frac{4\pi\mu^2}{Q^2}\right)^\epsilon \frac{1}{\Gamma(1-\epsilon)} \frac{T_R}{s_{13}} \left[T(Q^2 - s_{123} - s_{134}, s_{123}, s_{134}) \left(\frac{v^2 + (1-v)^2 - \epsilon}{(1-\epsilon)} \right) \right. \right. \\ &\quad \left. \left. - \frac{Q^2(Q^2 - s_{123} - s_{134})}{s_{123}s_{134}} 4 v(1-v) \left(2\cos^2\theta' - \frac{1}{(1-\epsilon)} \right) \right] \right\} \\ &\quad + \left\{ (1 \leftrightarrow 2) \right\} + \left\{ (3 \leftrightarrow 4) \right\} + \left\{ (1 \leftrightarrow 2)(3 \leftrightarrow 4) \right\} \quad . \quad (3.22) \end{aligned}$$

As a check on this result we notice that after integration over θ' the coefficient of the s_{13} pole is proportional to

$$P_{qG}^{n \neq 4}(v) = T_R \left(\frac{(v^2 + (1-v)^2 - \epsilon)}{(1-\epsilon)} \right) \quad , \quad (3.23)$$

which reduces to the normal Altarelli-Paris¹⁸⁾ function in the limit $\epsilon \rightarrow 0$.

Eqs. (3.17, 3.19 and 3.22) contain the singular part of the four-parton cross section as we approach the three-jet region. We therefore define

$$d\sigma^{(s)} = d\sigma_{I+II+III}^{(s)} \quad . \quad (3.24)$$

The two quantities in eq. (1.21) are now fully defined. Performing the first three integrations^(F5) in all the parts of eq. (3.24) and changing the names of the variables we may write^(F6)

$$\begin{aligned}
 \frac{1}{\sigma_0} d\sigma(s) &= H \frac{\alpha_s}{2\pi} C_F \left(\frac{4\pi\mu^2}{Q^2} \right)^\epsilon \frac{1}{\Gamma(1-\epsilon)} \frac{1}{Q^4} \int ds_{12} ds_{13} ds_{23} (y_{12} y_{13} y_{23})^{-\epsilon} \\
 &\quad \delta(Q^2 - s_{12} - s_{13} - s_{23}) T(s_{12}, s_{13}, s_{23}) \frac{\alpha_s}{2\pi} \frac{\Gamma(1-\epsilon)}{\Gamma(1-2\epsilon)} \left(\frac{4\pi\mu^2}{Q^2} \right)^\epsilon \\
 &\quad \left\{ \frac{1}{\epsilon} (2C_F + N_C) + \frac{1}{\epsilon} \left(3C_F - 2C_F \ell\pi y_{12} + \frac{11}{6} N_C + N_C \ell\pi \frac{y_{12}}{y_{13} y_{23}} - \frac{2}{3} T_R \right) \right. \\
 &+ C_F \left[\ell\pi^2 y_{12} - \ell\pi^2 y_{13} - \ell\pi^2 y_{23} - 2\text{Li}_2(1-y_{13}) - 2\text{Li}_2(1-y_{23}) + 7 - 3 \ell\pi y_{12} - \frac{3}{2} \ell\pi y_{13} - \frac{3}{2} \ell\pi y_{23} \right] \\
 &+ N_C \left[-\frac{3}{2} \ell\pi^2 y_{12} + \frac{1}{2} \ell\pi^2 y_{13} + \frac{1}{2} \ell\pi^2 y_{23} - 2\text{Li}_2(1-y_{12}) + \frac{67}{18} - \frac{11}{6} \ell\pi y_{13} - \frac{11}{6} \ell\pi y_{23} \right] \\
 &\left. T_R \left[\left(\frac{2}{3} \ell\pi y_{13} + \frac{2}{3} \ell\pi y_{23} - \frac{10}{9} \right) \right] \right\} \quad . \quad (3.25)
 \end{aligned}$$

Adding this to eq. (2.20) we obtain,

$$\begin{aligned}
 \frac{1}{\sigma_0} \frac{d\sigma(s) + d\sigma(3)}{dC} &= \frac{\alpha_s(Q^2)}{2\pi} C_F \frac{1}{Q^4} \int ds_{12} ds_{13} ds_{23} \delta(1-y_{12}-y_{13}-y_{23}) \delta(C - C^{(3)}(s_{12}, s_{13}, s_{23})) \\
 &\quad \left\{ T(s_{12}, s_{13}, s_{23}) \left[1 + \right. \right. \\
 &+ \frac{\alpha_s}{2\pi} C_F \left(\frac{2\pi^2}{3} - 1 - \ell\pi^2 y_{13} - \ell\pi^2 y_{23} - 2\text{Li}_2(1-y_{13}) - 2\text{Li}_2(1-y_{23}) - 3 \ell\pi y_{12} - \frac{3}{2} \ell\pi y_{13} - \frac{3}{2} \ell\pi y_{23} \right) \\
 &+ \frac{\alpha_s}{2\pi} N_C \left(\frac{\pi^2}{3} - \ell\pi^2 y_{12} - 2\text{Li}_2(1-y_{12}) + \frac{67}{18} - \frac{11}{6} \ell\pi y_{13} - \frac{11}{6} \ell\pi y_{23} \right) \\
 &\left. \left. + \frac{\alpha_s}{2\pi} T_R \left(\frac{2}{3} (\ell\pi y_{13} + \ell\pi y_{23}) - \frac{10}{9} \right) \right] + \frac{\alpha_s}{2\pi} F(s_{12}, s_{13}, s_{23}) \right\} \quad , \quad (3.26)
 \end{aligned}$$

where the function F is given in eq. (2.21). All poles have vanished in eq. (3.26) as they must and the limit $\epsilon \rightarrow 0$ has been taken. Eq. (3.26) can be evaluated by a simple numerical integration. The full C distribution is given by the sum of eq. (3.26) and the term,

$$\frac{1}{\sigma_0} d\sigma^{(4)} \delta(C - C^{(4)}) - d\sigma^{(s)} \delta(C - C^{(3)}) \quad . \quad (3.27)$$

Eq. (3.27) is completely finite except at $C = 0$ and hence may be evaluated in four dimensions. In the next section the numerical values of the distributions of the C and D distributions are discussed.

IV. Results

The numerical integration of the terms in eq. (3.26) and eq. (3.27) are treated separately since eq. (3.26) is a two-dimensional integration, (which we performed by ordinary numerical integration), whereas eq. (3.27) requires integration over five parameters and was integrated using a Monte Carlo technique which we describe below.

It was not practical to invert the expression for $C^{(4)}$ to use the delta function to eliminate one of the variables of integration. We therefore generated events, calculated the cross-sections $d\sigma^{(4)}$ and $d\sigma^{(s)}$ and binned them according to their values of $C^{(4)}$ and $C^{(3)}$ respectively. In general, the bins $C^{(4)}$ and $C^{(3)}$ do not coincide. However, in the infrared limit where four-jet events simulate three-jet events

$$C^{(4)} \xrightarrow{s_{ij} \rightarrow 0} C^{(3)} + O(s_{ij}^{1/2}), \quad (4.1)$$

(c.f., eq. (1.15)), so that in this region $d\sigma^{(4)}$ and its singular part $d\sigma^{(s)}$ are guaranteed to fall in the same bin and hence cancel. The approach of $C^{(4)}$ to $C^{(3)}$ is slow. Moreover $d\sigma^{(4)}$ and $d\sigma^{(s)}$ have double poles. There exist regions of phase space for which $C^{(4)}$ and $C^{(3)}$ lie in adjacent bins but where $d\sigma^{(4)}$ and $d\sigma^{(s)}$ are still large, thus adding a large contribution of one sign to one bin and a large contribution of the other sign to an adjacent bin. This causes fluctuations in our histograms which gradually decrease as the number of points is increased. Despite the fact that for the parts of the cross-section which contain double poles, over 10^6 points were taken, remnants of the e fluctuations can be seen in our histograms.

In Figs. 9,10,11 we present our results^(F8) for the quantity $\frac{C}{\sigma} \frac{d\sigma}{dC}$ for the group weights C_{FC}^N , C_{FR}^T and C_F^2 respectively. All three distributions display a discontinuity at $C = 3/4$. Above $C = 3/4$ the differential cross-section receives

contributions from $d\sigma^{(4)}$ only; these contributions diverge as $C \rightarrow 3/4$ from above, as we approach the point where four jets coalesce to three. At the point $C = 3/4$ and for all points $C < 3/4$ this divergence is cancelled by $d\sigma^{(5)}$. For $C > 3/4$ the cross-section is constrained to be positive; for $C < 3/4$ the distributions, Figs. 9, 10, 11, are higher order corrections to the lower order distribution, Fig. 3, and may therefore be negative as in Fig. 10. The leading log behavior (c.f., eq. 3.26) around $C = 0^{8,20}$ is visible in Fig. 11.

$$\frac{d\sigma}{dC} \Big| \sim \frac{\alpha_s}{2\pi} \frac{\ell_{\pi} C}{C} \left(1 - \frac{\alpha_s}{2\pi} 2 C_F \ell_{\pi}^2 C \right) . \quad (4.2)$$

However by comparison with Figs. 9, 10, we see that only at extremely low values of C is this leading log behavior the dominant effect. We have no way of calculating the distribution in the first bin since it contains divergences which are cancelled by the $O(\alpha_s^2)$ contributions to two-jet processes (proportional to a delta function at the origin). We can use the total cross-section^{15,16}, now known up to $O(\alpha_s^2)$, to calculate what the average value in this bin should be. Since the correction to the total cross-section is small, but the correction for $C > 0.05$ is large, a sizeable negative contribution is required in the first bin to balance it.

From our figures we can calculate the fraction of events which lie in the range $1/2 < C < 1$. This gives a measure of the multijet events (see Fig. 1). Our numerical estimate is,

$$\frac{1}{\sigma} \int_{1/2}^1 \frac{d\sigma}{dC} dC = 2.8 \left(\frac{\alpha_s(Q^2)}{2\pi} \right) \left[1 + K \left(\frac{\alpha_s(Q^2)}{2\pi} \right) \right] , \quad (4.3)$$

where,

$$K = 36.5 \pm 0.5 . \quad (4.4)$$

By choosing the range $1/2 \leq C \leq 1$ we have excluded the pure two-jet region and also the perturbative two-jet events which are promoted to higher values of C

by hadronization. Choosing a notional value of

$$\frac{\alpha_s(Q^2)}{2\pi} \sim 0.03 \quad Q = 30 \text{ GeV}, \Lambda = 0.5 \text{ GeV} \quad , \quad (4.5)$$

we see that the perturbation series in eq. (4.5) does not appear to converge.

Our conclusion is that the multijet fraction of e^+e^- hadronic events calculated in the $\overline{\text{MS}}$ renormalization prescription does not give a convergent perturbation series despite the fact that the total e^+e^- cross section leads to a well-behaved perturbation series in this renormalization scheme. The problem of isolating and resumming the large terms is complicated by the fact that we do not have an analytic answer for the whole cross-section. Moreover in the piece for which we do have an analytic expression (eq. (3.26)), several large terms contribute to the overall large effect. Not all the terms have the same sign, so that by resumming one piece we may destroy a cancellation and aggravate the situation rather than improve it. In view of these difficulties, we limit ourselves to certain tentative suggestions.

In eq. (2.24) we noted the appearance of π^2 terms related to the soft singularity. Since the soft logarithms exponentiate it is presumably true that the π^2 terms also exponentiate. Under this assumption eq. (4.5) becomes

$$\frac{1}{\sigma} \int_{1/2}^1 \frac{d\sigma}{dC} dC \sim \exp \frac{\alpha_s(Q^2)}{2\pi} \left(C_F + \frac{N_C}{2}\right) \pi^2 \quad 2.8 \left(\frac{\alpha_s(Q^2)}{2\pi}\right) \left(1 + 9 \frac{\alpha_s(Q^2)}{2\pi}\right) . \quad (4.6)$$

After extraction of the exponential, the remaining correction at PETRA energies would be in the perturbative range. To illustrate this point we have plotted in Fig. 12 the total $O(\alpha_s^2)$ correction to $\frac{C}{\sigma} \frac{d\sigma}{dC}$, together with the $O(\alpha_s)$ contribution (Fig. 3) multiplied by a factor $\left(\frac{\alpha_s}{2\pi} \left(C_F + \frac{N_C}{2}\right) \pi^2\right)$. Independent of any exponentiation hypotheses, Fig. 13 shows that the shape of the distribution is not substantially altered for values of $0.3 < C < 0.75$.

Eq. (3.26) also contains terms of the form

$$\frac{\alpha_s}{2\pi} \left(\frac{2}{3} T_R - \frac{11}{6} N_C \right) \ell_{\tilde{n}}(y_{13}y_{23}) \quad . \quad (4.7)$$

whose physical origin is that the four momentum squared which determines the strength of the quark gluon coupling is not Q^2 but a smaller number. The running coupling constant should therefore be evaluated not at Q^2 but at Q^2 multiplied by a possibly C-dependent factor chosen to cancel as closely as possible the effect of the terms in eq. (4.7).

It appears that a reliable perturbative estimate for the fraction of multijet events will require a detailed understanding of the infrared singularities and the mass singularities, leading and subleading logs together with associated terms.

In Fig. 13 we have plotted the total $\frac{d\sigma}{dD}$ vs. D and its breakup into the group weight factors C_F^2 , $C_F N_C$, $C_F T_R$. The bulk of the cross-section is contained in the "QED-like" piece proportional to C_F^2 . (The same is true for $\frac{Cd\sigma}{\sigma dC}$ in the purely four-jet region $C > 3/4$, whereas for $C < 3/4$ the C_F^2 and $C_F N_C$ pieces are of similar size.) Whilst we cannot compare directly because we calculate different quantities our results are in qualitative agreement with Ref. 10.

Finally we have calculated the average values of C and D.

$$\langle C \rangle = \left(\frac{\alpha_s}{2\pi} \right) C_F (4\pi^2 - 33) \left(1 + 17 \frac{\alpha_s}{2\pi} \right) \quad (4.8)$$

$$\langle D \rangle = \left(\frac{\alpha_s}{2\pi} \right)^2 60.5 \quad (4.9)$$

These average values are very sensitive to the effects of hadronization.

V. Conclusions

We have calculated the α_s^2 corrections to event shapes in e^+e^- annihilation using the perturbation theory of massless quarks and gluons and neglecting the fragmentation of these partons into final state hadrons. The results have been presented in terms of differential cross-sections with respect to C and D. The double differential cross-section in C and D completely specifies the distribution in the eigenvalue plot (Fig. 1), and hence the shape of the event. In order to obtain results which were free from infrared divergences it was necessary to calculate both the one-loop correction to the cross-section for a three-parton final state and the tree diagram cross-section for the production of four partons.

After integration of the four-jet cross-section, both of the above contributions contain double and single poles. The potentially singular parts of the four-parton cross-section are easily recognizable since they are proportional to a lower order three-jet cross-section folded with the appropriate Altarelli-Parisi kernel. However in addition to these pieces the four-jet cross section contains singular terms not proportional to Altarelli-Parisi kernels which after integration contribute at the level of subleading logs. This confirms that the leading pole approximation can be used to obtain the coefficient of the leading but not the subleading logs. This, of course, does not alter the status of the KLN theorem; the infrared divergences of the two parts still cancel.

The histogram obtained for the differential cross-section $\frac{C}{\sigma} \frac{d\sigma}{dC}$ displays such a large correction over the $O(\alpha_s)$ distribution that doubt is cast on the validity of the perturbation expansion. However over a large range of C $0.3 \leq C \leq 0.75$ this large correction is dominated by a π^2 which arises from a mismatch in the above-mentioned cancellation of double poles; the one-loop diagrams generate a $\ln^2(-Q^2)$ and the four particle cross-section has a $\ln^2(Q^2)$ with opposite sign. . There is reason to believe that these π^2 terms

can be summed to all orders giving a large exponential factor multiplying a convergent perturbation series. As we have emphasized in the previous section this procedure of selecting one of the large terms and resumming it is scarcely justifiable.

Notwithstanding this convergence problem, we find a large $O(\alpha_s^2)$ contribution to the differential cross section away from the two-jet region $C = 0$. The $O(\alpha_s^2)$ correction to the total cross-section on the other hand is small eq. (2.16), so that the large corrections for $C \neq 0$ must be balanced by a large correction of opposite sign at $C = 0$.

Before these results may be compared with experimental data, the effects of hadronization should be taken into account. Hadronization is the process by which quarks and gluons arrange themselves into color singlet states by exchanging soft quarks and gluons. Logical consistency requires that the program of hadronization implemented when parton bremsstrahlung is taken into account should differ from that applied to the bare quark-antiquark jets, otherwise we run the risk of double counting. The converse of this statement is that the final state interactions which we calculate represent the first primitive (non-confining) steps in the hadronization. Since the effects of hadronization fall like a power of the energy and the effects we calculate vanish only logarithmically there must exist an energy for which the perturbation series in $\alpha_s(Q^2)$ is a faithful approximation to QCD. At present energies we know that the hadronization will introduce significant smearing effects. In particular the large negative correction at $C = 0$, when smeared out will reduce the calculated corrections for $C > 0$. This smearing of perturbative two-jet events should change only low values of C and the effects of hadronization at large values of C should be much less spectacular. If this hope is vindicated, and if the

large contributions to the perturbation series can indeed be summed, we would expect a much larger multijet fraction, defined by making a lower cutoff on C , than previously estimated.

We are pleased to acknowledge useful discussions with R. P. Feynman, R. D. Field, T. Goldman, Z. Kunszt, H. D. Politzer, and S. Wolfram. We thank the MATHLAB at MIT for the use of MACSYMA.

Appendix A

In this appendix we give the values of the harder integrals used in the calculation. The first integral is required to isolate the singular piece of the four jet cross-section which contains a double pole.

$$I(x,y) = \int_0^x ds s^{-1-\epsilon} \int_0^1 dv \frac{v^{-\epsilon}(1-v)^{-\epsilon}}{(s+(y-s)v)}$$

$$I(x,y) = \frac{\Gamma^2(1-\epsilon)}{\Gamma(1-2\epsilon)} \frac{1}{y} \left[\frac{1}{2\epsilon^2} - \frac{\ell_n y}{2\epsilon} - \frac{1}{2} \ell_n^2 \frac{x}{y} + \frac{1}{4} \ell_n^2 y - \text{Li}_2(1-\frac{x}{y}) + O(\epsilon) \right] \quad (\text{A.1})$$

The remaining two integrals are required for the calculation of the one loop corrections to the three jet cross-section. Setting $Q^2 = (p_1+p_2+p_3)^2$ we have²¹⁾,

$$\int \frac{d^n k}{(2\pi)^n} \frac{1}{k^2(k-p_2)^2(k+p_3)^2(k+p_1+p_3)^2}$$

$$= \frac{i}{16\pi^2} \left(-\frac{4\pi}{Q^2} \right)^\epsilon \frac{\Gamma(1+\epsilon)\Gamma^2(1-\epsilon)}{\Gamma(1-2\epsilon)} \frac{2}{s_{13}s_{23}} \left[\frac{1}{\epsilon^2} - \frac{1}{\epsilon} \ell_n (y_{13}y_{23}) \right. \\ \left. + \frac{1}{2} \ell_n^2 y_{13} + \frac{1}{2} \ell_n^2 y_{23} + R(y_{13},y_{23}) + O(\epsilon) \right] \quad (\text{A.2})$$

where $R(x,y)$ is given in eq. (2.22). Lastly, we have,

$$\int \frac{d^n k}{(2\pi)^n} \frac{k \cdot p_1 k \cdot p_2}{(k+p_1)^2(k-p_2)^2(k+p_1+p_3)^2}$$

$$= \frac{i}{16\pi^2} \left(-\frac{4\pi}{Q^2} \right)^\epsilon \frac{\Gamma(1+\epsilon)\Gamma^2(1-\epsilon)}{\Gamma(2-2\epsilon)} \left\{ -\frac{1}{\epsilon} \left[\frac{s_{12}^2 s_{13}^2 \ell_n y_{12}}{4(s_{13}+s_{23})^3} \right. \right. \\ \left. \left. + \frac{s_{13}^2 s_{23}^2 + s_{13}^2 s_{23} + s_{12}(s_{13}^2 - 2s_{13}s_{23} - s_{23}^2)}{8(s_{13} + s_{23})^2} \right] + \frac{s_{12}s_{13}s_{23}}{4(s_{13} + s_{23})^2} \right. \\ \left. + \frac{s_{12}^2 \ell_n y_{12}(s_{13}^2 \ell_n y_{12} + s_{23}^2 + s_{13}^2 + 4s_{13}s_{23})}{8(s_{13} + s_{23})^3} + O(\epsilon) \right\} \quad (\text{A.3})$$

Appendix B

In this appendix we present the differential cross-section calculated in order α_s^2 for the production of a four parton final state. The reaction $e^+e^- \rightarrow q\bar{q}GG$ gives a contribution,

$$\begin{aligned} \frac{1}{\sigma_0} d\sigma^{(4)} &= C_F \left(\frac{\alpha_s}{2\pi} \right)^2 \frac{Q^2}{2} \int dy_{123} \int dy_{134} \int dy_{13} \Theta(y_{13}) \Theta(y_{123}y_{134} - y_{13}) \\ &\quad \Theta(y_{13} + 1 - y_{123} - y_{134}) \int_0^1 dv \frac{1}{\pi} \int_0^\pi d\theta' \\ &\quad \left\{ (A + B + C) + (1 \rightleftharpoons 2) + (3 \rightleftharpoons 4) + (1 \rightleftharpoons 2, 3 \rightleftharpoons 4) \right\} \end{aligned} \quad (B.1)$$

The reaction $e^+e^- \rightarrow \bar{q}\bar{q}qq$ gives the contribution,

$$\begin{aligned} \frac{1}{\sigma_0} d\sigma^{(4)} &= C_F \left(\frac{\alpha_s}{2\pi} \right)^2 \frac{Q^2}{4} \int dy_{123} \int dy_{134} \int dy_{13} \Theta(y_{13}) \Theta(y_{123}y_{134} - y_{13}) \\ &\quad \Theta(y_{13} + 1 - y_{123} - y_{134}) \int_0^1 dv \frac{1}{\pi} \int_0^\pi d\theta' \\ &\quad \left\{ (D + E) + (1 \rightleftharpoons 2) + (3 \rightleftharpoons 4) + (1 \rightleftharpoons 2, 3 \rightleftharpoons 4) \right\} \end{aligned} \quad (B.2)$$

where the quantities v and θ' are defined by eqs.(3.2-3.5). The quantities A,B,C,D and E are given in the following equations. Our results for the matrix element for the first reaction are in agreement with the results of Ali et al. (ref.10) except for typing error which will be corrected in the published version of their paper.

$$A = C_F \left\{ (s_{12}s_{34}^2 - s_{13}s_{24}s_{34} + s_{14}s_{23}s_{34} + 3s_{12}s_{23}s_{34} + 3s_{12}s_{14}s_{34} + 4s_{12}^2s_{34} - s_{13}s_{23}s_{24} + 2s_{12}s_{23}s_{24} - s_{13}s_{14}s_{24} - 2s_{12}s_{13}s_{24} + 2s_{12}^2s_{24} + s_{14}s_{23}^2 + 2s_{12}s_{23}^2 + s_{14}^2s_{23} + 4s_{12}s_{14}s_{23} + 4s_{12}^2s_{23} + 2s_{12}s_{14}^2 + 2s_{12}s_{13}s_{14} + 4s_{12}^2s_{14} + 2s_{12}^2s_{13} + 2s_{12}^3) / (2s_{13}s_{134}s_{234}s_{24}) + (s_{24}s_{34} + s_{12}s_{34} + s_{13}s_{24} - s_{14}s_{23} + s_{12}s_{13}) / (s_{13}s_{134}^2) + 2s_{23}(Q^2 - s_{13}) / (s_{13}s_{134}s_{24}) + s_{34} / (2s_{13}s_{24}) \right\} \quad (B.3)$$

$$B = (C_F - N_C/2) \left\{ (s_{12}s_{24}s_{34} + s_{12}s_{14}s_{34} - s_{13}s_{24}^2 + s_{13}s_{14}s_{24} + 2s_{12}s_{14}s_{24}) / (s_{13}s_{134}s_{23}s_{14}) + s_{12}(Q^2 + s_{34})s_{124} / (s_{134}s_{234}s_{14}s_{24}) - (2s_{13}s_{24} + s_{14}^2 + s_{13}s_{23} + 2s_{12}s_{13}) / (s_{13}s_{134}s_{14}) + s_{12}s_{123}s_{124} / (2s_{13}s_{14}s_{23}s_{24}) \right\} \quad (B.4)$$

$$C = N_C \left\{ -(5s_{12}s_{34}^2 + 2s_{12}s_{24}s_{34} + 2s_{12}s_{23}s_{34} + 2s_{12}s_{14}s_{34} + 2s_{12}s_{13}s_{34} + 4s_{12}^2s_{34} - s_{13}s_{24}^2 + s_{14}s_{23}s_{24} + s_{13}s_{23}s_{24} + s_{13}s_{14}s_{24} - s_{12}s_{14}s_{24} - s_{13}^2s_{24} - 3s_{12}s_{13}s_{24} - s_{14}s_{23}^2 - s_{14}^2s_{23} + s_{13}s_{14}s_{23} - 3s_{12}s_{14}s_{23} - s_{12}s_{13}s_{23}) / (4s_{134}s_{234}s_{34}^2) + (3s_{12}s_{34}^2 - 3s_{13}s_{24}s_{34} + 3s_{12}s_{24}s_{34} + 3s_{14}s_{23}s_{34} - s_{13}s_{24}^2 - s_{12}s_{23}s_{34} + 6s_{12}s_{14}s_{34} + 2s_{12}s_{13}s_{34} - 2s_{12}^2s_{34} + s_{14}s_{23}s_{24} - 3s_{13}s_{23}s_{24} - 2s_{13}s_{14}s_{24} + 4s_{12}s_{14}s_{24} + 2s_{12}s_{13}s_{24} + 3s_{14}s_{23}^2 + 2s_{14}^2s_{23} + 2s_{14}^2s_{12} + 2s_{12}^2s_{14} + 6s_{12}s_{14}s_{23} - 2s_{12}s_{13}^2 - 2s_{12}^2s_{13}) / (4s_{13}s_{134}s_{234}s_{34}) + (2s_{12}s_{34}^2 - 2s_{13}s_{24}s_{34} + s_{12}s_{24}s_{34} + 4s_{13}s_{23}s_{34} + 4s_{12}s_{14}s_{34} + 2s_{12}s_{13}s_{34} + 2s_{12}^2s_{34} - s_{13}s_{24}^2 + 3s_{14}s_{23}s_{24} + 4s_{13}s_{23}s_{24} - 2s_{13}s_{14}s_{24} + 4s_{12}s_{14}s_{24} + 2s_{12}s_{13}s_{24} + 2s_{14}s_{23}^2 + 4s_{13}s_{23}^2 + 2s_{13}s_{14}s_{23} + 2s_{12}s_{14}s_{23} + 4s_{12}s_{13}s_{23} + 2s_{12}^2s_{14} + 4s_{12}^2s_{13} + 4s_{12}s_{13}s_{14} + 2s_{12}^2s_{14}) / (4s_{13}s_{134}s_{24}s_{34}) - (s_{12}s_{34}^2 - 2s_{14}s_{24}s_{34} - 2s_{13}s_{24}s_{34}$$

(continued)

$$\begin{aligned}
 & - s_{14} s_{23} s_{34} + s_{13} s_{23} s_{34} + s_{12} s_{14} s_{34} + 2s_{12} s_{13} s_{34} - 2s_{14}^2 s_{24} - 4s_{13} s_{14} s_{24} \\
 & - 4s_{13}^2 s_{24} - s_{14}^2 s_{23} - s_{13}^2 s_{23} + s_{12} s_{13} s_{14} - s_{12} s_{13}^2) / (2s_{13} s_{34} s_{134}^2) \\
 & + (s_{12} s_{34}^2 - 4s_{14} s_{24} s_{34} - 2s_{13} s_{24} s_{34} - 2s_{14} s_{23} s_{34} - 4s_{13} s_{23} s_{34} - 4s_{12} s_{14} s_{34} \\
 & - 4s_{12} s_{13} s_{34} - 2s_{13} s_{14} s_{24} + 2s_{13}^2 s_{24} + 2s_{14}^2 s_{23} - 2s_{13} s_{14} s_{23} - s_{12} s_{14}^2 \\
 & - 6s_{12} s_{13} s_{14} - s_{12} s_{13}^2) / (4s_{34}^2 s_{134}^2) \}
 \end{aligned} \tag{B.5}$$

$$\begin{aligned}
 D = T_R \left\{ \left[(s_{13} s_{23} s_{34} + s_{12} s_{23} s_{34} - s_{12}^2 s_{34} + s_{13} s_{23} s_{24} + 2s_{12} s_{23} s_{24} - s_{14} s_{23}^2 \right. \right. \\
 + s_{12} s_{13} s_{24} + s_{12} s_{14} s_{23} + s_{12} s_{13} s_{14}) / (s_{13}^2 s_{123}^2) - (s_{12} s_{34}^2 - s_{13} s_{24} s_{34} \\
 + s_{12} s_{24} s_{34} - s_{14} s_{23} s_{34} - s_{12} s_{23} s_{34} - s_{13} s_{24}^2 + s_{14} s_{23} s_{24} - s_{13} s_{23} s_{24} \\
 \left. \left. - s_{13}^2 s_{24} + s_{14} s_{23}^2) / (s_{13}^2 s_{123} s_{134}) \right] + \left[(1 \leftrightarrow 3, 2 \leftrightarrow 4) \right] \right\}
 \end{aligned} \tag{B.6}$$

$$\begin{aligned}
 E = (C_F - N_C/2) \left\{ \left[(s_{12} s_{23} s_{34} - s_{12} s_{24} s_{34} + s_{12} s_{14} s_{34} + s_{12} s_{13} s_{34} + s_{13} s_{24}^2 \right. \right. \\
 - s_{14} s_{23} s_{24} + s_{13} s_{23} s_{24} + s_{13} s_{14} s_{24} + s_{13}^2 s_{24} - s_{14} s_{23}^2 - s_{14}^2 s_{23} - s_{13} s_{14} s_{23}) / \\
 (s_{13} s_{23} s_{123} s_{134}) - s_{12} (s_{12} s_{34} - s_{23} s_{24} - s_{13} s_{24} - s_{14} s_{23} - s_{14} s_{13}) / \\
 (s_{13} s_{23} s_{123}^2) - (s_{14} + s_{13}) (s_{24} + s_{23}) s_{34} / (s_{13} s_{23} s_{134} s_{234}) \left. \right] \\
 + \left[(1 \leftrightarrow 3, 2 \leftrightarrow 4) \right] \}
 \end{aligned} \tag{B.7}$$

References

1. S. Orito, JADE Collaboration, Proc. Int. Symp. on Lepton and Photon Interactions at High Energies (FNAL, Batavia, 1979);
D. P. Barber et al., Mark-J Collaboration, Phys. Rev. Lett. 43, (1979) 830;
Ch. Berger et al., PLUTO Collaboration, Phys. Lett. 86B (1979) 418;
R. Brandelik et al., TASSO Collaboration, Phys. Lett. 86B (1979) 243.
2. J. Ellis, M. K. Gaillard and G. G. Ross, Nucl. Phys. B111 (1976) 253;
(E: 130 (1977) 516).
3. C. L. Basham, L. S. Brown, S. D. Ellis, and S. T. Love, Phys. Rev. D17
(1978) 2298; Phys. Rev. Lett. 41 (1978) 1585;
H. Georgi and M. Machacek, Phys. Rev. Lett. 39 (1977) 1237;
E. Fahri, Phys. Rev. Lett. 39 (1977) 1587;
A. De Rújula, J. Ellis, E. G. Floratos and M. K. Gaillard, Nucl. Phys. B138
(1978) 387;
S. Y. Pi, F. L. Jaffe and F. E. Low, Phys. Rev. Lett. 41 (1978) 142;
S. S. Shei, Phys. Lett. 79B (1978) 245;
K. Shizuya and S.-H. H. Tye, Phys. Rev. Lett. 41 (1978) 1195;
T. A. DeGrand, Y. J. Ng and S.-H. H. Tye, Phys. Rev. D16 (1977) 3251.
4. G. C. Fox and S. Wolfram, Phys. Rev. Lett. 41 (1978) 1581; Nucl. Phys. B149
(1979) 413; Phys. Lett. B82 (1979) 134.
5. G. Sterman and S. Weinberg, Phys. Rev. Lett. 39 (1977) 1436.
6. G. Parisi, Phys. Lett. 74B (1978) 65.
7. J. F. Donoghue, F. E. Low and S. Y. Pi, Phys. Rev. D20 (1979) 2759
8. S. L. Wu and G. Zobernig, Z. Physik C2 (1979) 107.
9. T. Kinoshita, J. Math. Phys. 3 (1962) 650;
T. D. Lee and M. Nauenberg, Phys. Rev. 133 (1964) 1549.

10. A. Ali, J. G. Körner, Z. Kunszt, J. Willrodt, G. Schierholz and E. Pietarinen, Phys. Lett. 82B (1979) 285 and DESY report 79/54 (1979), also Nucl. Phys. B. (in press);
K. J. F. Gaemers and J. A. M. Vermaseren, CERN preprint TH 2816.
11. G. 't Hooft and M. Veltman, Nucl. Phys. B44 (1972) 189;
C. G. Bollini and J. J. Giambiagi, Nuovo Cim. 12B (1972) 20;
W. J. Marciano, Phys. Rev. D12 (1975) 3861.
12. A. E. Terrano and S. Wolfram, Caltech report in preparation; see also S. Wolfram, "MACSYMA Tools for Feynman Diagram Calculation," in Proc. 1979 MACSYMA Users' Conference (ed. V. E. Lewis), Washington 1979; Caltech preprint CALT-68-736.
13. MATHLAB Group, M.I.T. Laboratory for Computer Science, 'MACSYMA Primer,' (March 1978) and 'MACSYMA Reference Manual,' Version 9 (Dec. 1977).
14. W. A. Bardeen, A. J. Buras, D. W. Duke, T. Muta, Phys. Rev. D18 (1978) 3998.
15. T. Appelquist and H. Georgi, Phys. Rev. D8 (1973) 4000;
A. Zee, Phys. Rev. D8 (1973) 4038.
16. M. Dine and J. Sapiirstein, Phys. Rev. Lett. 43, 668 (1979);
W. Celmaster and R. J. Gonsalves, UCSD Preprint-10P10-206, 207 (1979);
K. G. Chetyrkin, A. L. Kataev and F. V. Tkachov, Phys. Lett. 85B, 277 (1979).
17. W. Caswell, Phys. Rev. Lett. 33 (1974) 244;
D. R. T. Jones, Nucl. Phys. B75 (1974) 531.
18. G. Altarelli and G. Parisi, Nucl. Phys. B126 (1977) 298;
G. Parisi, Proc. 11th Rencontre de Moriond, 1976, ed., J. Tran Thanh Van.
19. W. Furry, Phys. Rev. 51 (1937) 125.
20. P. Binétruy, Phys. Lett. 91B (1980) 245.
21. K. Fabricius and I. Schmitt, Z. Phys. C3 (1979) 51.

Footnotes

1. This tensor differs from the tensor used by Wu and Zobernig (Ref. 8) which is not linear in collinear momenta. Their tensor is not finite in QCD perturbation theory.
2. The factors of $1/3$ and $1/27$ are included so the variables span the range from 0 to 1.
3. The four-jet reactions, eqs. (2.3, 2.4) have also been considered in Ref. 10 and DeGrand, Ng and Tye, (Ref. 3).
4. In the following equations we have dropped integrable square root singularities.
5. This is permissible because $C^{(3)}$ in the delta function is independent of these variables and therefore gives no constraint.
6. One of the integrals required is given in Appendix A.
7. In our notation this corresponds to the interchanges $1 \rightarrow 3$, $3 \rightarrow 4$, $2 \rightarrow 1$, $4 \rightarrow 2$ in eqs. (3.2 - 3.5).
8. In these plots σ is the total cross section, eq. (2.16) corrected to order α_s (and not σ_0).

Figure Captions

1. Eigenvalue plot showing lines of constant C and constant D. By imposing $C > \frac{1}{2}$ we exclude the two-jet region. For $\lambda_1 > \lambda_2 > \lambda_3$ only the top right-hand triangle is populated.
2. (a) The reaction $\gamma^* \rightarrow q + \bar{q}$
 (b,c) The reaction $\gamma^* \rightarrow q + \bar{q} + G$.
3. Plot of $\frac{Cd\sigma}{\sigma_0 dC}$ (in units of $\frac{\alpha_s}{2\pi}$) vs. C.
4. Virtual corrections to the process $\gamma^*(Q) \rightarrow q + \bar{q} + G$. Diagrams 12 to 19 are contributions to wave function renormalization. Corrections to the gluon wave function involving ghosts or the four-gluon vertex and similar in structure to graphs 18 and 19 have not been shown.
5. Diagrams contributing to the process $\gamma^* \rightarrow q\bar{q}GG$.
6. Transition probabilities for the process $\gamma^* \rightarrow q\bar{q}GG$. On-shell particles are indicated by the short cutting line and the numbers refer to the momentum labels. All the other transition probabilities can be obtained by permutation of momentum labels.
7. Diagrams contributing to the process $\gamma^* \rightarrow q\bar{q} q\bar{q}$. Diagrams which differ only by the exchange of identical final state fermions have a relative minus sign.
8. Transition probabilities for the process $\gamma^* \rightarrow q\bar{q} q\bar{q}$. On-shell particles are indicated by a short cutting line and the numbers refer to the momentum labels. All other transition probabilities can be obtained by exchange of momentum labels.

9. The part of the $O(\alpha_s^2)$ correction to $\frac{Cd\sigma}{\sigma dC}$ containing the Casimirs $C_F N_C$ is plotted in units of $\left(\frac{\alpha_s}{2\pi}\right)^2$ against the variable C.
10. The part of the $O(\alpha_s^2)$ correction to $\frac{Cd\sigma}{\sigma dC}$ containing the Casimirs $C_F T_R$ is plotted in units of $\left(\frac{\alpha_s}{2\pi}\right)^2$ against the variable C. The number of flavors is set equal to 5.
11. The part of the $O(\alpha_s^2)$ correction to $\frac{Cd\sigma}{\sigma dC}$ containing the Casimirs C_F^2 is plotted in units of $\left(\frac{\alpha_s}{2\pi}\right)^2$ against the variable C.
12. The total $\frac{Cd\sigma}{\sigma dC}$ vs. C (solid line). The lower order $\frac{Cd\sigma}{\sigma dC}$ (Fig. 3) multiplied by $\left(\frac{\alpha_s}{2\pi}\right)(2C_F + N_C)\pi^2$ vs. C (dashed line). Both are plotted in units of $\left(\frac{\alpha_s}{2\pi}\right)^2$.
13. $\frac{1}{\sigma} \frac{d\sigma}{dD}$ in units of $\left(\frac{\alpha_s}{2\pi}\right)^2$ plotted against D. The total is shown (solid line) together with C_F^2 part (dashed), $C_F N_C$ (dotted), $C_F T_R$ (dash-dotted).

Group weight Permutation of first row	Class A C_F^2				Class B $C_F \left(C_F - \frac{N_C}{2} \right)$				Class C $C_F N_C$				
	B11	B32	B21	B22	B42	B52	B53	B41	B71	B72	B82	B77	B87
(3 ↔ 4)	B44	B65	B54	B55	B51	-	B62	-	B74	B75	B85	-	-
(1 ↔ 2)	-	-	B64	B66	B61	-	-	-	B84	B86	B76	B88	-
(1 ↔ 2) (3 ↔ 4)	-	-	B31	B33	B43	B63	-	-	B81	B83	B73	-	-

Table 1: The interchange table relating the graphs for $e^+e^- \rightarrow q\bar{q}GG$.

Group weight Permutation of first row	Class D $C_F T_R$			Class E $C_F(C_F - \frac{N_C}{2})$						Class F C_F		
	A77	A88	A87	A83	A76	A73	A86	A84	A75	A81	A82	A53
(1 ↔ 2)	A55	A66	A65	A61	A85	A51	-	A62	-	A63	A64	A71
(3 ↔ 4)	A33	A44	A43	A74	A32	-	A42	-	A31	A54	-	-
(1 ↔ 2) (3 ↔ 4)	A11	A22	A21	A52	A41	-	-	-	-	A72	-	-

Table 2: The interchange table relating the graphs for $e^+e^- \rightarrow \bar{q}q\bar{q}q$.

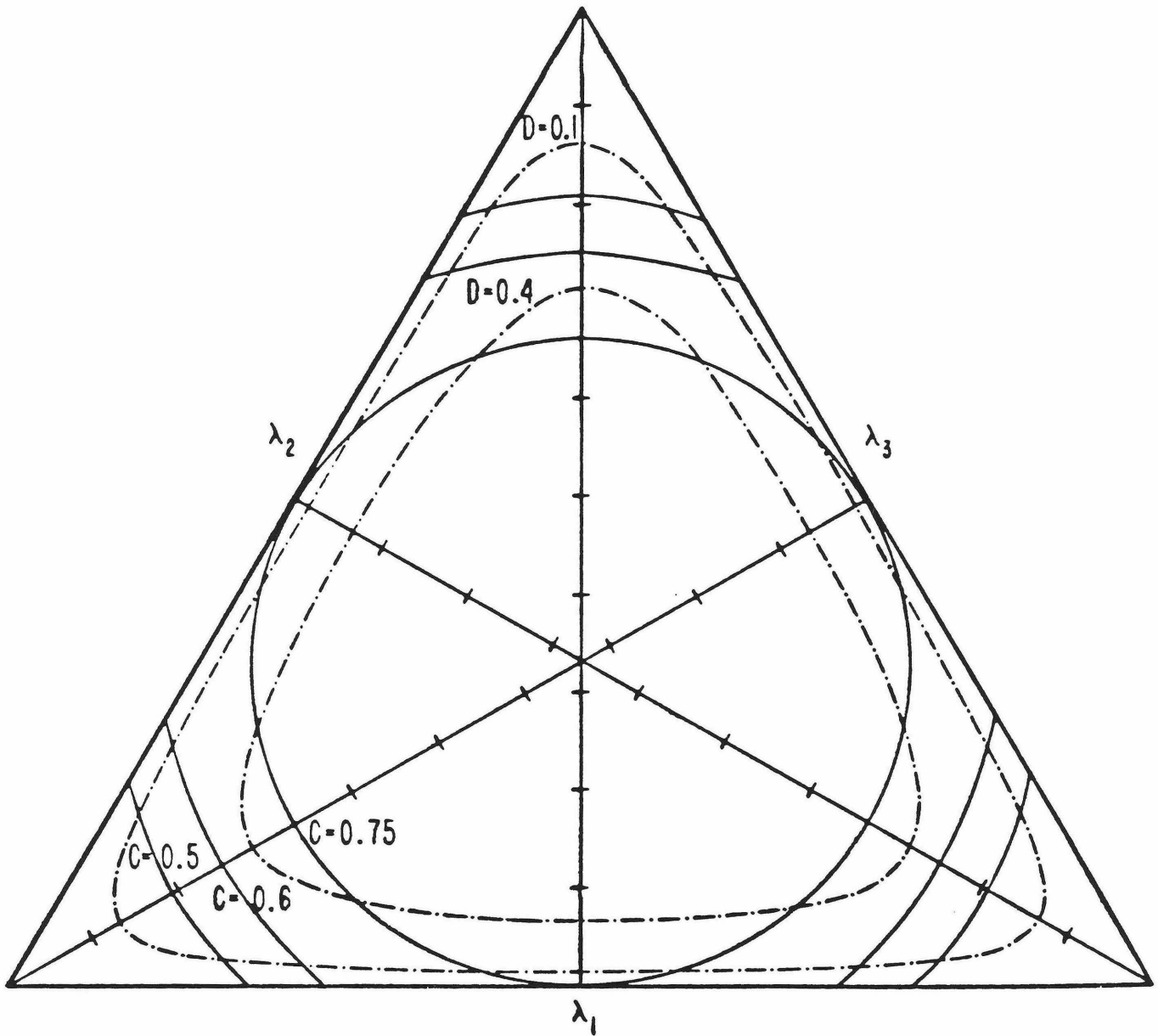


Fig. 1

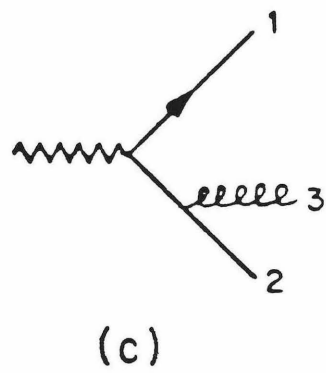
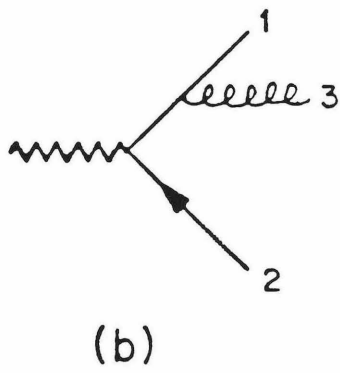
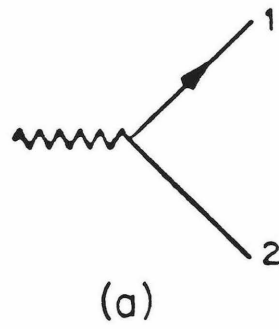


Fig. 2

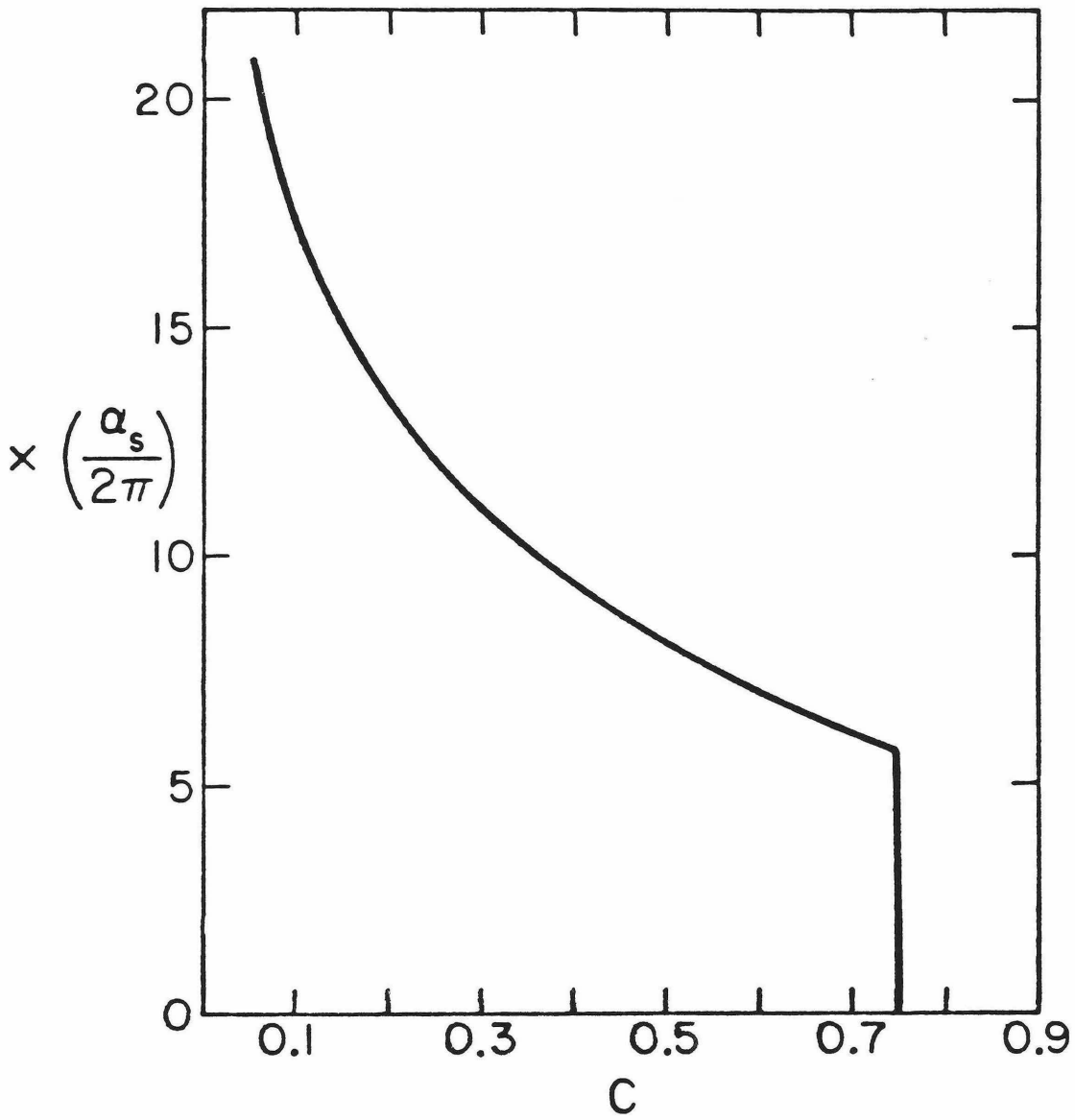


Fig. 3

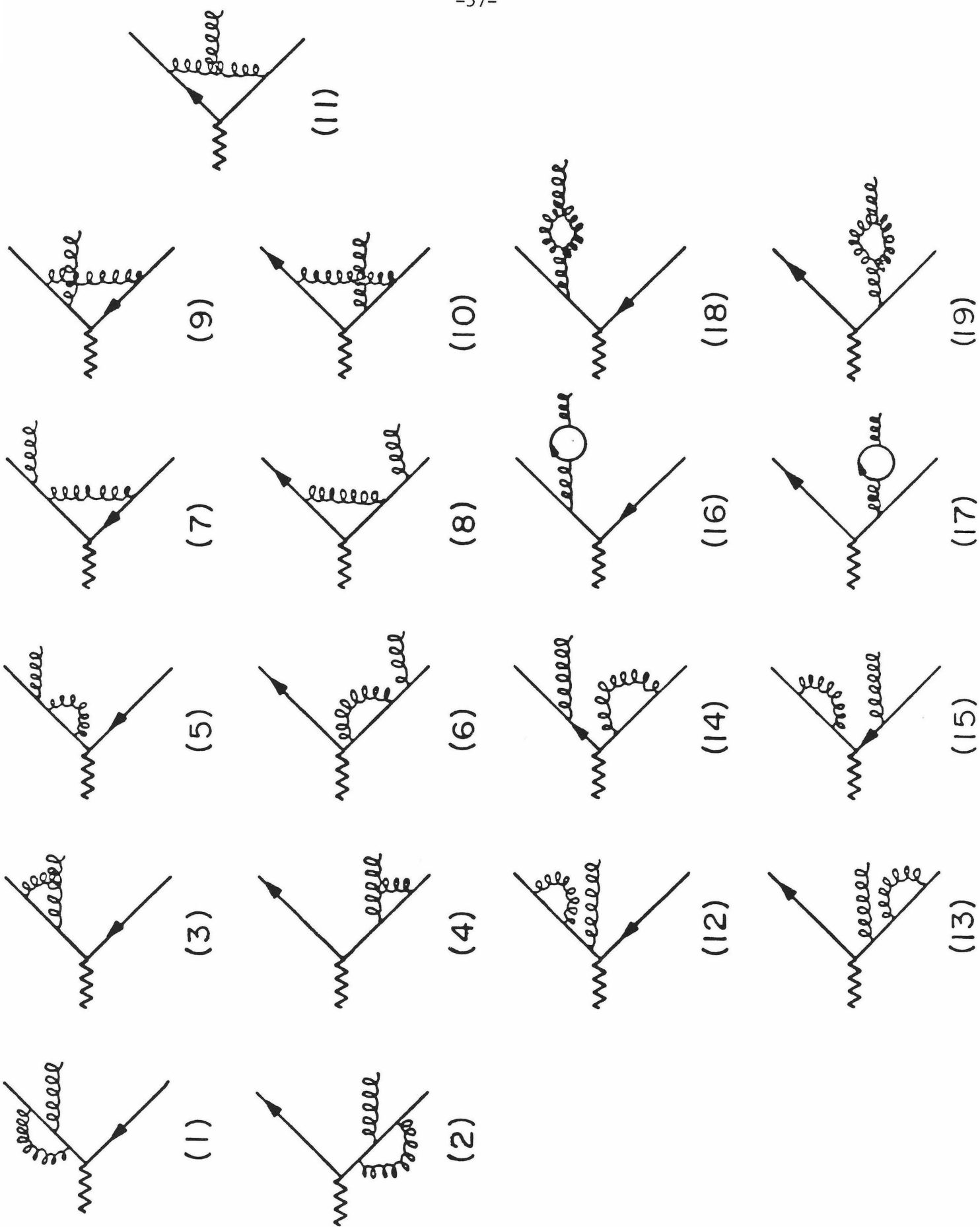


Fig. 4

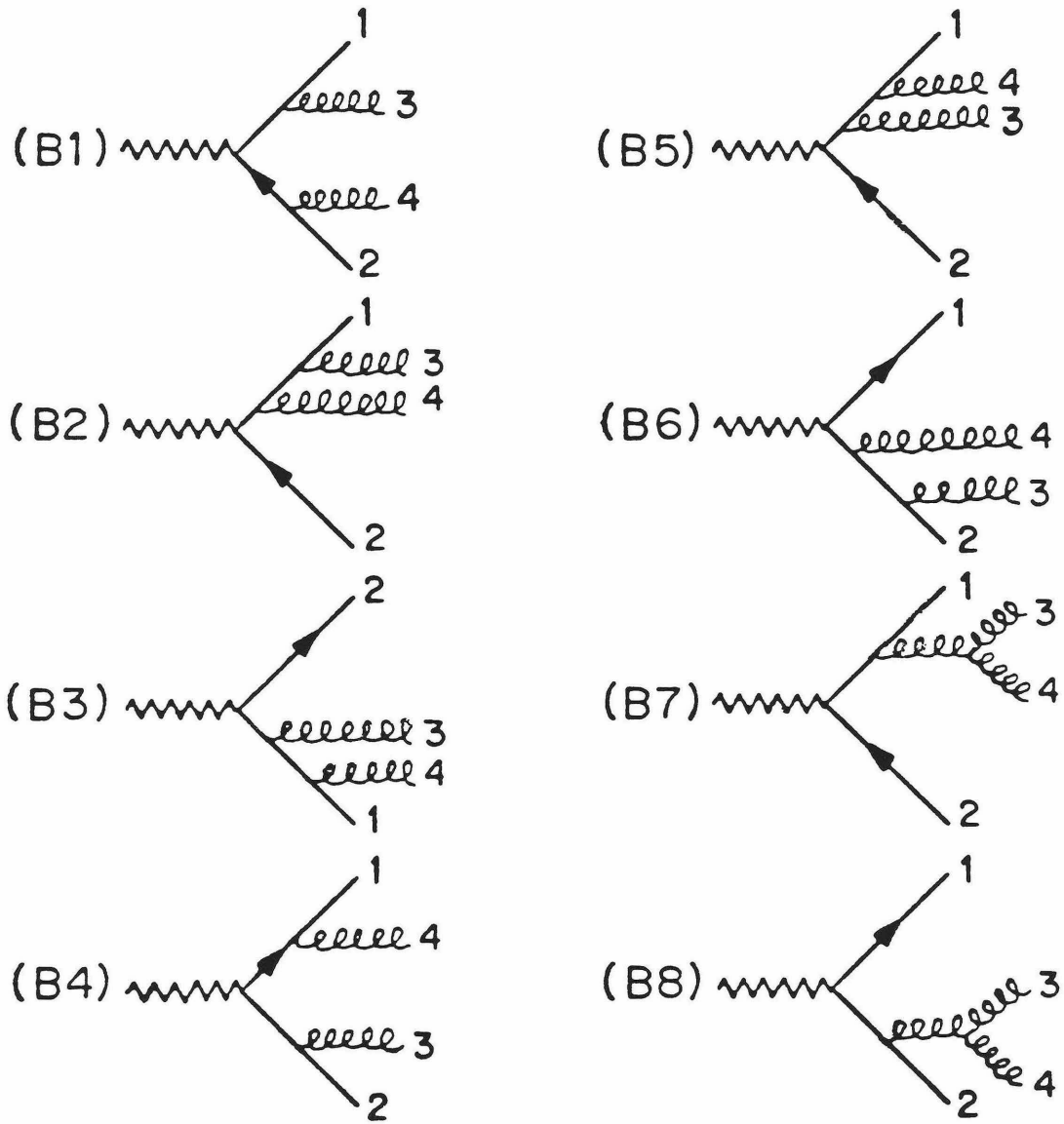
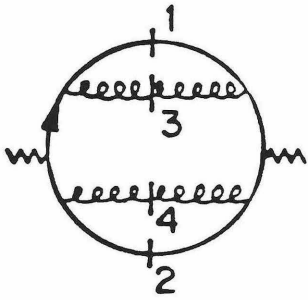
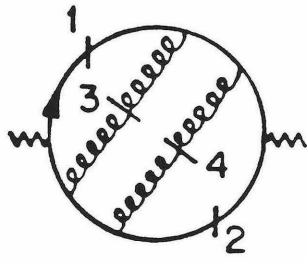


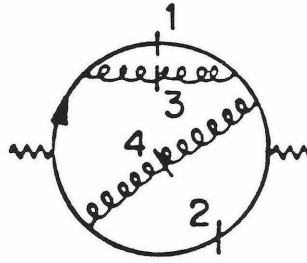
Fig. 5



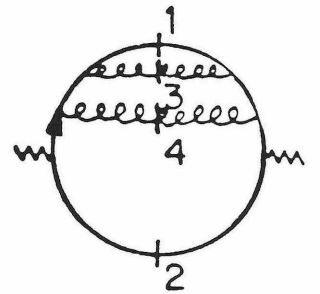
B11



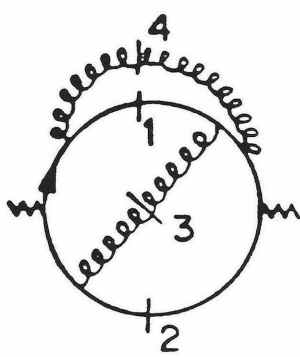
B32



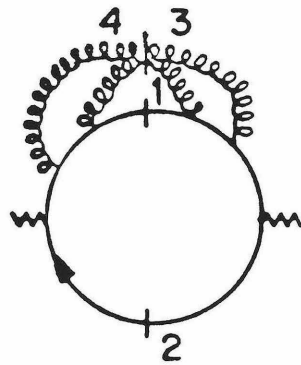
B21



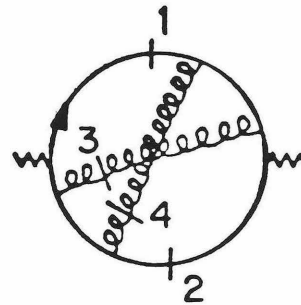
B22



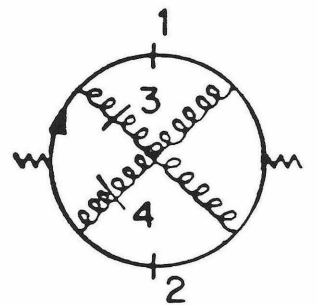
B42



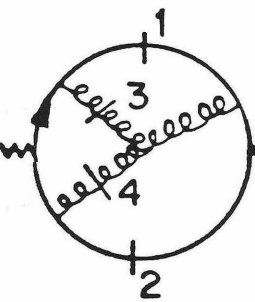
B52



B53



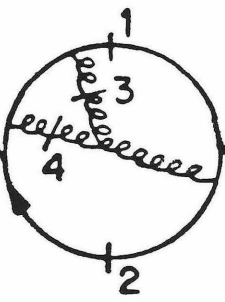
B41



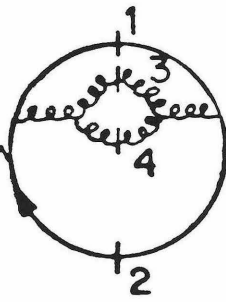
B71



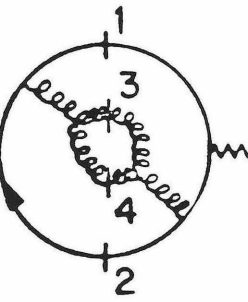
B72



B82



B77



B87

Fig. 6

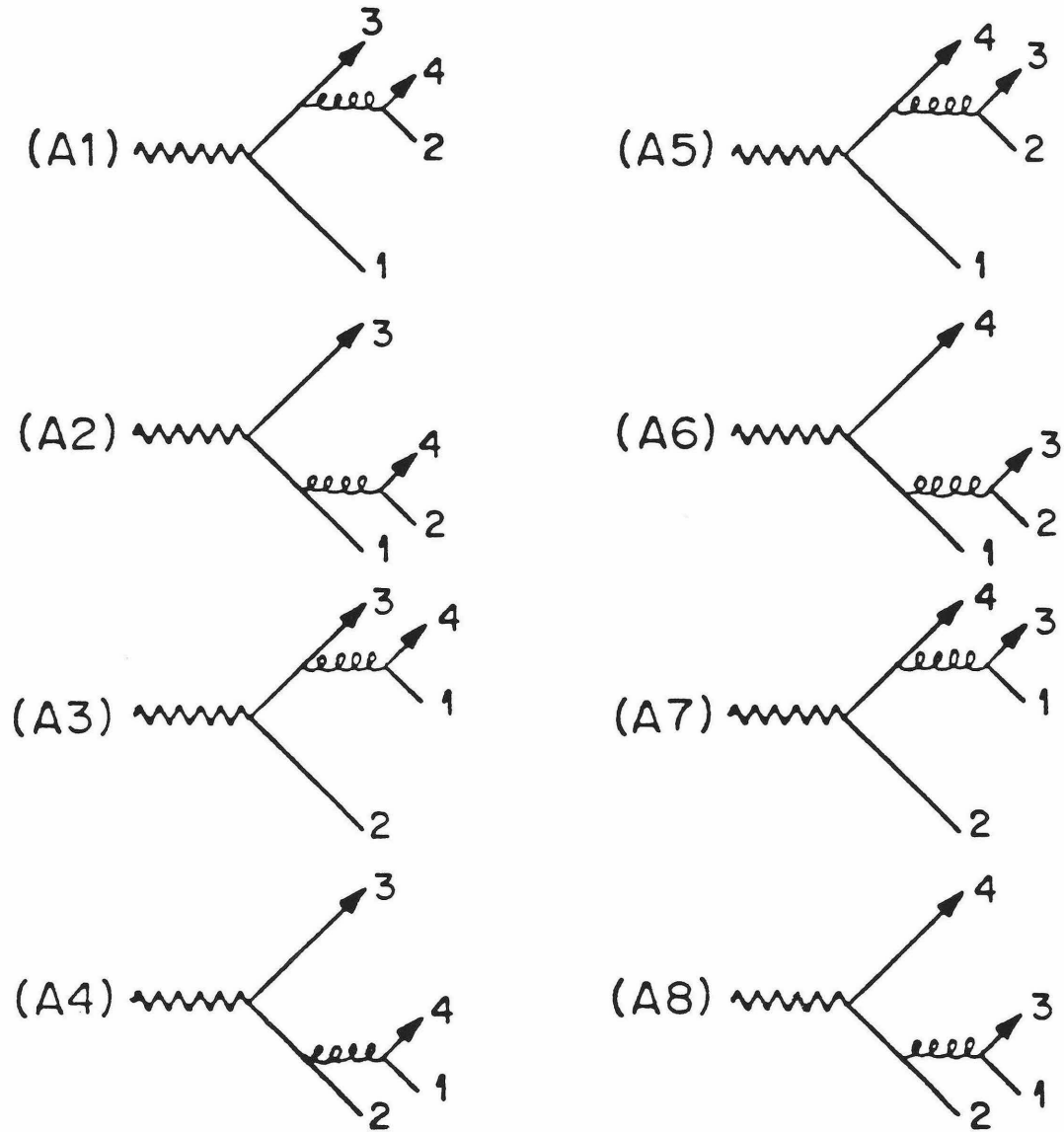
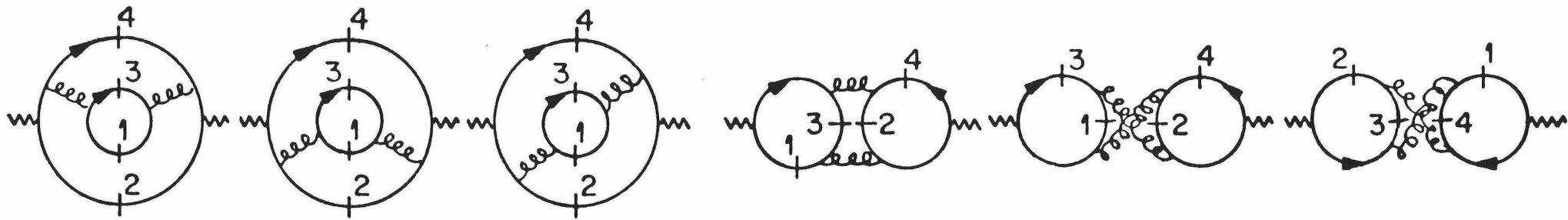


Fig. 7



A77

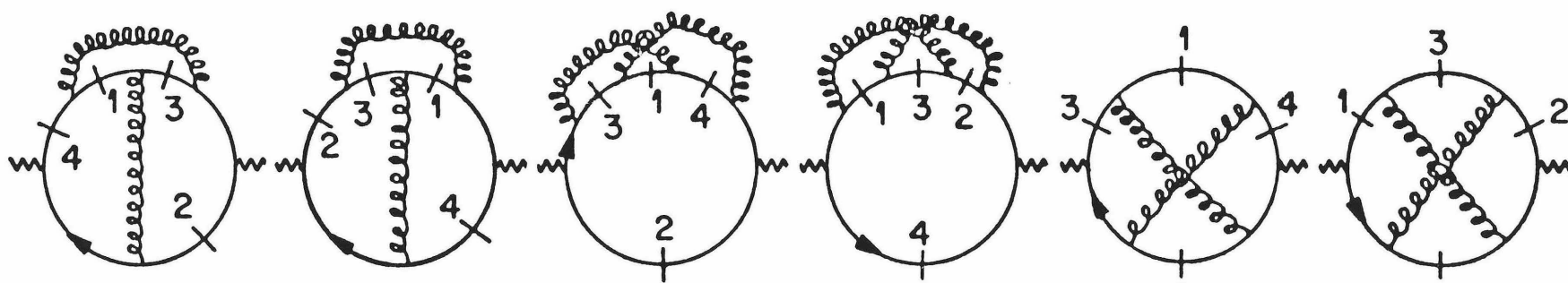
A88

A87

A81

A82

A53



A83

A76

A73

A86

A84

A75

Fig. 8

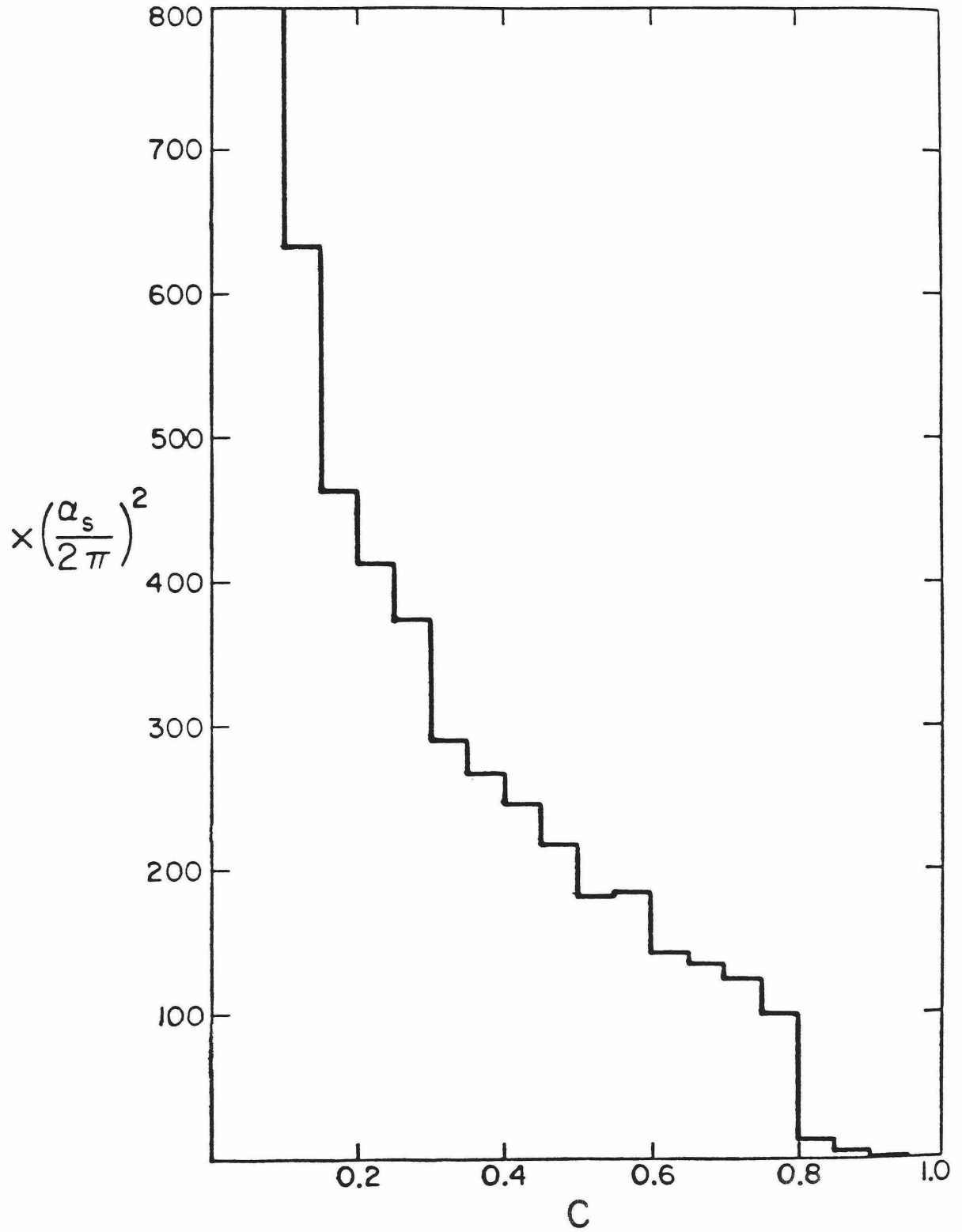


Fig. 9

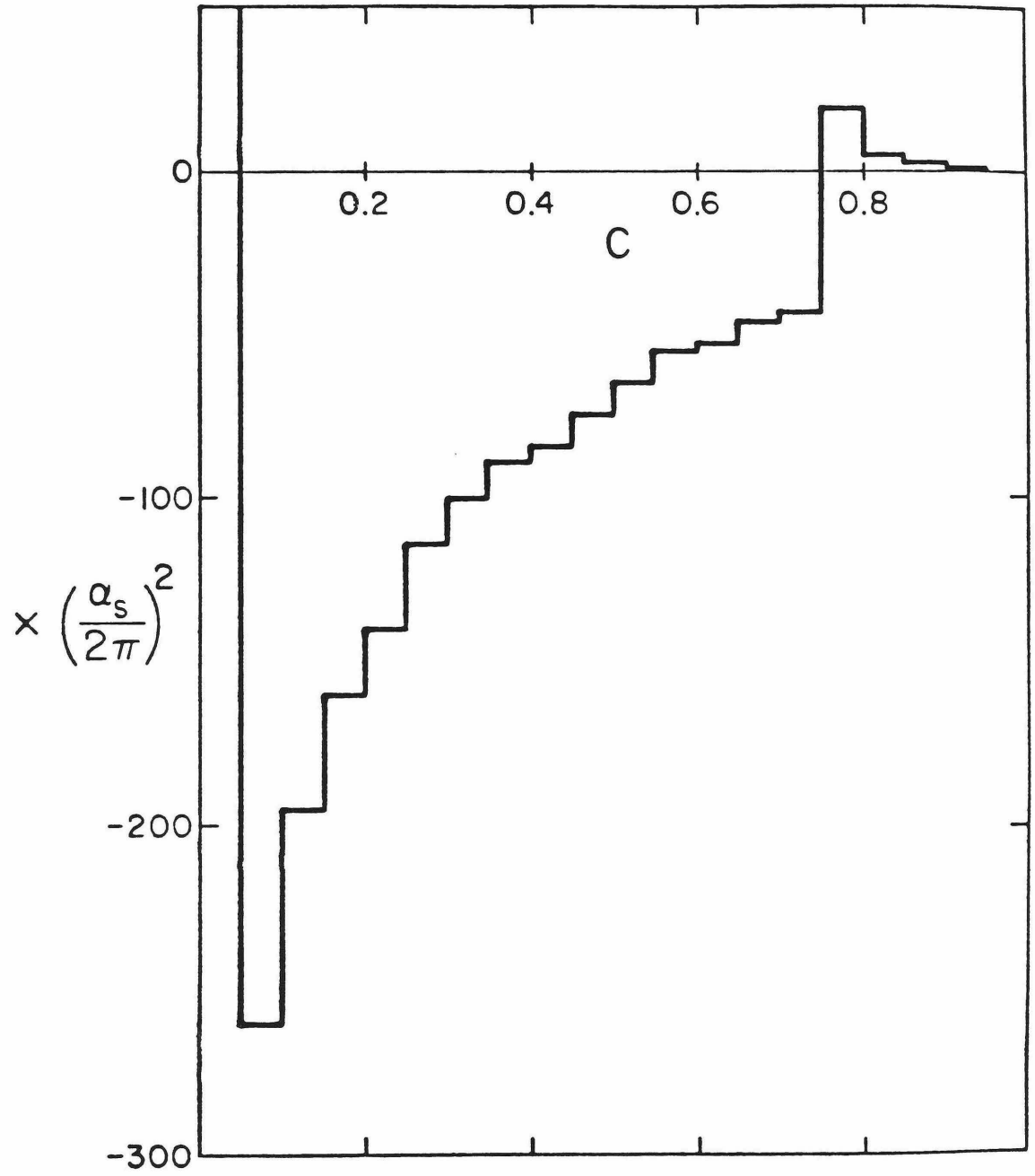


Fig. 10

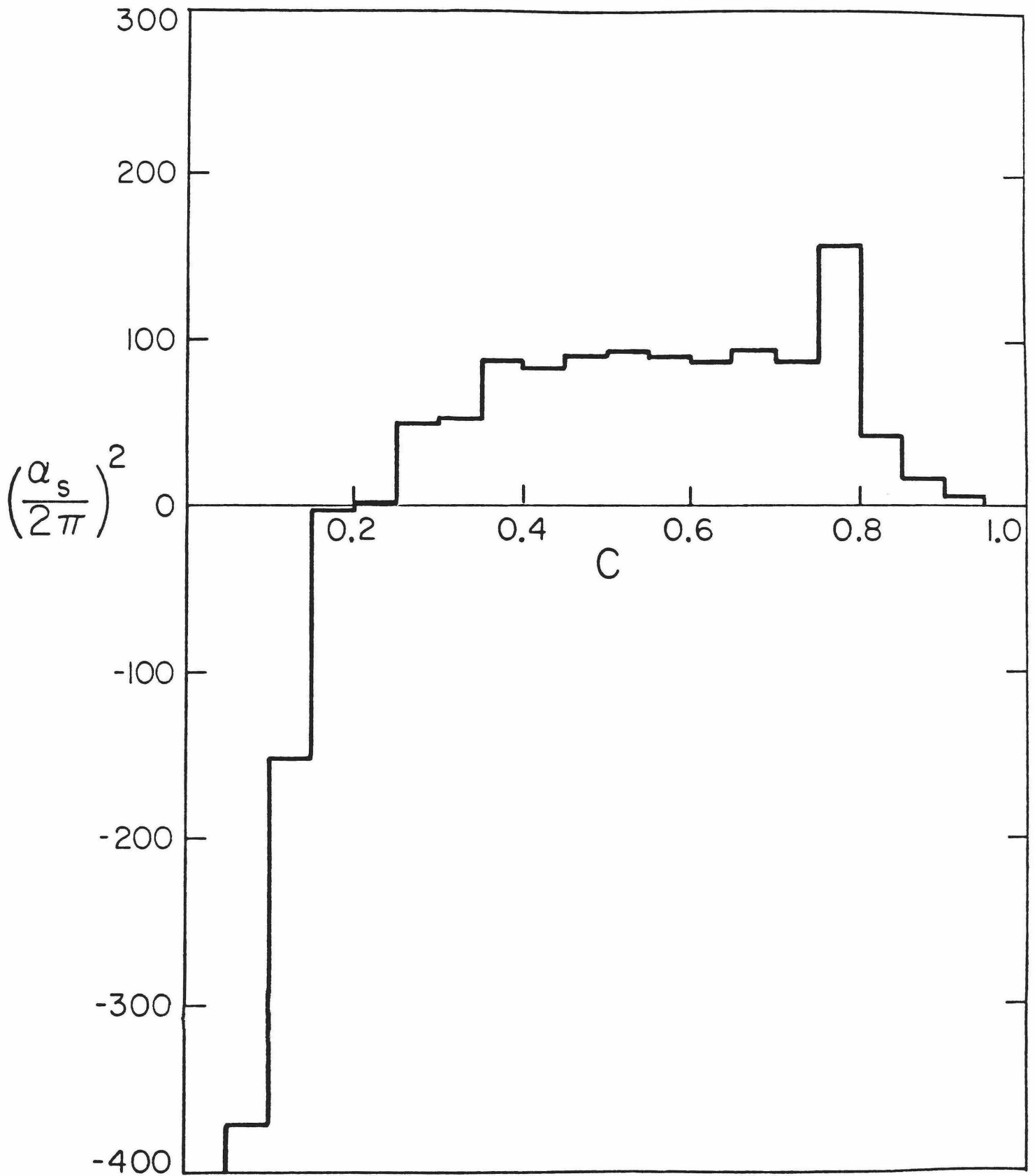


Fig. II

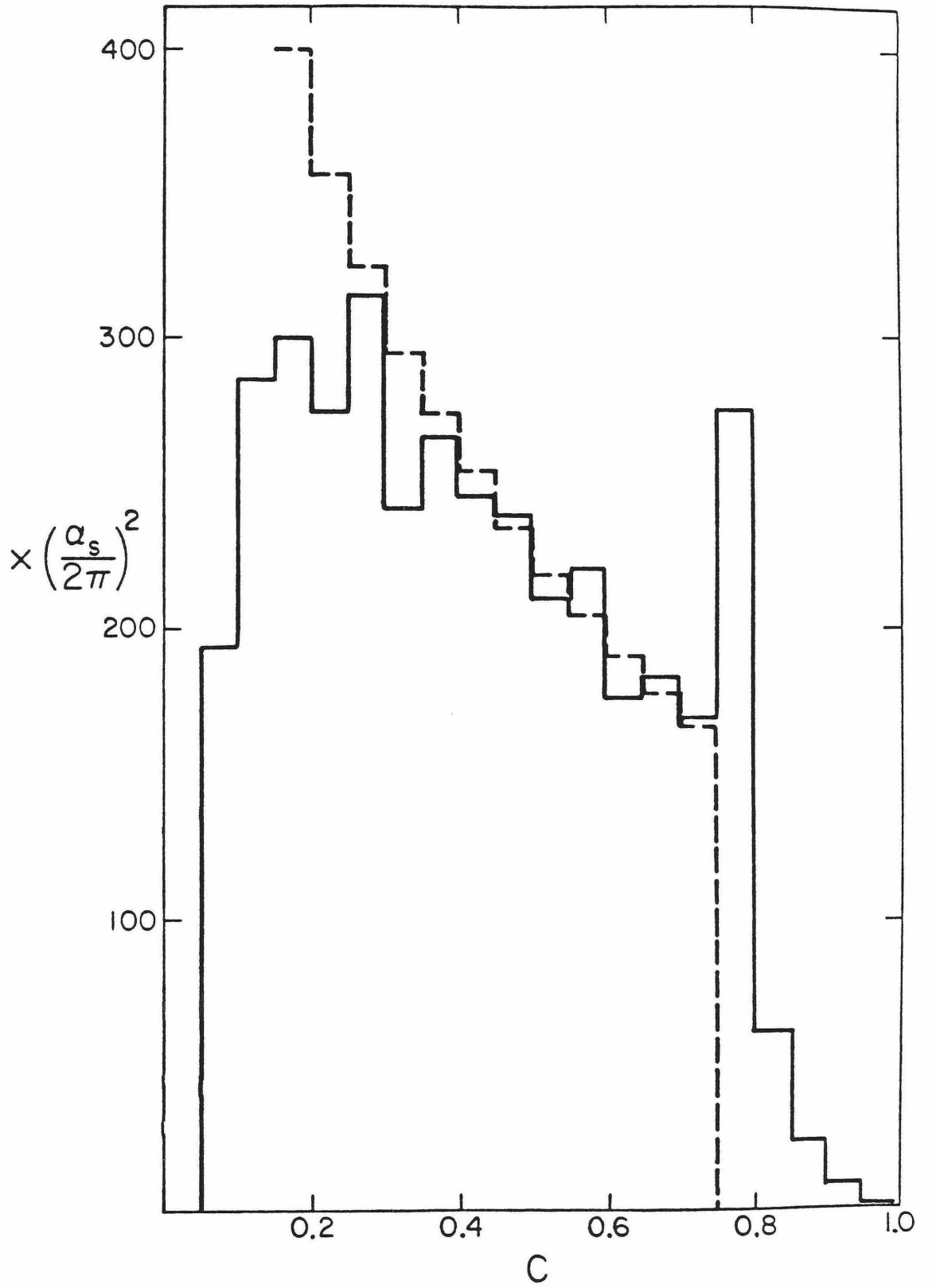


Fig. 12

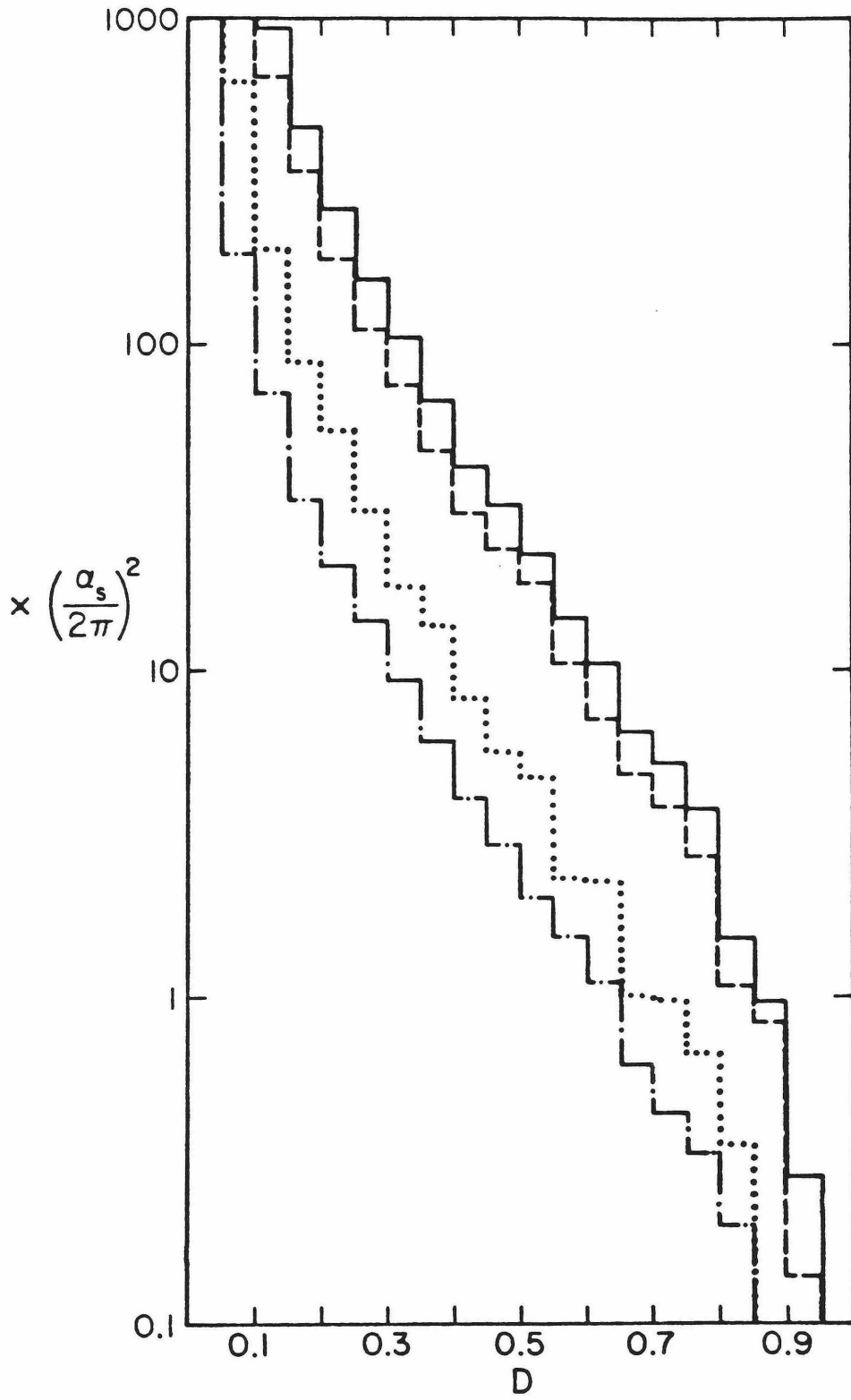


Fig. 13

4. A Method of Feynman Diagram Evaluation

The divergences encountered in higher order perturbative calculations in QCD cannot easily be handled by the techniques developed for QED. Gauge invariance and the simple Ward identities which result can be used to minimize the number and difficulty of the ultraviolet divergent integrals occurring in many QED calculations [fn 1]. In QCD the generalized Ward identities are complicated in covariant gauges^[3]. While they remain simple in axial gauges, the gluon propagator now becomes complicated, involving (nk) denominators in addition to k^2 ones^[4]. The simple regularization of soft infrared divergences in QED provided by giving the photon a small fictitious mass cannot be carried over to QCD^[5]. In addition, QCD contains collinear infrared divergences due to the existence of massless colored particles^[6]. The only known gauge invariant method for regularizing this abundance of divergences is to analytically continue the momentum integrals to $n = 4-2\epsilon$ dimensional space^[7].

The standard method of Feynman parametrization is economical only when a loop contains two lines. In this case the integration is done by applying the result (or its parametric derivatives):

$$\int \frac{d^n p}{(p-k_1)^{2\alpha_1} (p-k_2)^{2\alpha_2}} = \frac{1}{[(k_1-k_2)^2]^{\alpha_1+\alpha_2-2+\epsilon}} \frac{\Gamma(\alpha_1+\alpha_2-2+\epsilon)}{\Gamma(\alpha_1) \Gamma(\alpha_2)} \int_0^1 dx \frac{x^{\alpha_1-1} (1-x)^{\alpha_2-1}}{[x(1-x)]^{\alpha_1+\alpha_2-2+\epsilon}}$$

$$= \frac{1}{[(k_1-k_2)^2]^{\alpha_1+\alpha_2-2+\epsilon}} \frac{\Gamma(\alpha_1+\alpha_2-2+\epsilon)}{\Gamma(\alpha_1) \Gamma(\alpha_2)} \frac{\Gamma(2-\alpha_1-\epsilon)\Gamma(2-\alpha_2-\epsilon)}{\Gamma(4-\alpha_1-\alpha_2-2\epsilon)}$$

(1)

If more than two propagators are involved in a single loop, this procedure leads to difficult parametric integrals involving hypergeometric functions and their

parametric derivatives, the polylogarithms $Li_n(x)$ [8].

In this letter I describe a method of performing loop integrations in n dimensions which avoids Feynman parametrization.

We begin by transforming each loop momentum into hyperspherical coordinates [fn 2], thus separating the angular and radial integrations. The angular integrals are performed by first expanding each propagator in the series [9][fn 3]:

$$\frac{1}{[(p-q)^2]^\rho} = \frac{1}{(p^2 - 2p \cdot q + q^2)^\rho} = \frac{1}{(|p||q|)^\rho} \frac{\Gamma(\lambda)}{\Gamma(\rho)} \sum_{j=0}^{\infty} \frac{(j+\lambda)\Gamma(j+\rho)}{\Gamma(\lambda+j+1)} (T(p,q))^{j+\rho} \times {}_2F_1(\rho-\lambda, \rho+j; \lambda+j+1; (T(p,q))^2) C_j^\lambda(\hat{p} \cdot \hat{q}) \quad (2)$$

where the C_j^λ are the $n=2\lambda+2$ dimensional hyperspherical harmonics (Gegenbauer polynomials), and $T(p,q) = \min(\frac{|p|}{|q|}, \frac{|q|}{|p|})$. The properties of the C_j^λ are summarized in Table 1 [10,11]. When $n=3$ the C_j^λ become the Legendre polynomials, while when $n=4$ they are the Chebyshev polynomials $C_j^1(\cos\theta) = \frac{\sin(j+1)\theta}{\sin\theta}$. Some useful Gegenbauer expansions are given in Table 2 [10]. By expanding the hypergeometric functions in the usual power series ${}_2F_1(a,b,c;z) = \frac{\Gamma(c)}{\Gamma(a)\Gamma(b)} \sum_{j=0}^{\infty} \frac{\Gamma(j+a)\Gamma(j+b)}{j!\Gamma(j+c)} z^j$, the radial integrations become trivial. The resulting expression is then expanded around $\epsilon = 0$, which generally makes the final summations simple.

As an example, consider the simple scalar diagram in Fig. 1:

$$I = \int d^n p \, d^n q \frac{1}{p^4 (p-k)^2 (p-q)^2 q^2}$$

The angular integration is:

$$\int d\Omega_p d\Omega_q C_{m_1}^\lambda(\hat{p}\cdot\hat{k}) C_{m_2}^\lambda(\hat{p}\cdot\hat{q}) = \left[\frac{2\pi^{\lambda+1}}{\Gamma(\lambda+1)} \right]^2 \delta_{m_1 m_2} \delta_{m_1 0}$$

The radial integral is then:

$$\begin{aligned} I &= \frac{4\pi^{4-2\epsilon}}{\Gamma^2(2-\epsilon)} \int p^{3-2\epsilon} dp q^{3-2\epsilon} dq \frac{1}{p^4 q^2} \left(\frac{T(p,q)}{pq} {}_2F_1(\epsilon, 1; 2-\epsilon; T^2(p,q)) \right) \\ &\quad \times \left(\frac{T(p,q)}{pk} {}_2F_1(\epsilon, 1; 2-\epsilon; T^2(p,k)) \right) \\ &= \frac{4\pi^{4-2\epsilon}}{(k^2)^{1+2\epsilon}} \frac{1}{\Gamma^2(\epsilon)} \sum_{\substack{j=0 \\ j'=0}}^{\infty} \frac{\Gamma(j+\epsilon)\Gamma(j'+\epsilon)}{\Gamma(j+2-\epsilon)\Gamma(j'+2-\epsilon)} \left[\frac{(2j+1)(2j'+1)}{4(j+\epsilon)(j-\epsilon+1)(j'-2\epsilon)(j'+2\epsilon+1)} \right] \end{aligned}$$

It is clear that if neither j nor j' vanish, I is $O(\epsilon^2)$; if one of them vanishes I is $O(1)$ and if both vanish it has a double pole. Expanding around $\epsilon=0$, we get

$$I = \frac{\pi^{4-2\epsilon}}{(k^2)^{1+2\epsilon}} \left[-\frac{1}{2\epsilon^2} + \frac{2\gamma-1}{2\epsilon} + \frac{\zeta(2) - 2\gamma^2 + 2\gamma - 3}{2} \right]$$

($\gamma \approx 0.5772$ is Euler's constant). While this integral is sufficiently simple that it could have been done using only Eq. 1, it illustrates all aspects of the method, which has been used to calculate 3-loop diagrams with no trivial (i.e., using Eq. 1) subintegrations (Fig. 2).

One may also take the Fourier transform of a diagram and perform the Gegenbauer expansion in configuration space^[11]. Thus for the scalar diagram in Fig. 3:

$$\int d^n p d^n q \frac{1}{p^2 (p-k)^2 (p-q)^2 (q-k)^2 q^2} \propto \int d^n x d^n y d^n z \frac{e^{ik \cdot z}}{[x^2]^\lambda [y^2]^\lambda [(x-y)^2]^\lambda [(x-z)^2]^\lambda [(y-z)^2]^\lambda}$$

Since the generating function for the Gegenbauer polynomials is

$$(t^2 - 2tx + 1)^{-\lambda} = \sum_{j=0}^{\infty} t^j C_j^\lambda(x)$$

the expansion of the propagators is simple:

$$\frac{1}{[(x-y)^2]^\lambda} = \frac{1}{[x^2 - 2x \cdot y + y^2]^\lambda} = \sum_{j=0}^{\infty} \frac{[T(x,y)]^{j+\lambda}}{(|x||y|)^\lambda} C_j^\lambda(\hat{x} \cdot \hat{y})$$

However, the expansion of the exponential is also required, introducing Bessel functions into the final radial integral. In addition, if some of the momentum space propagators have ε -dependent exponents [fn 4], the choice of the origin in configuration space is constrained, possibly requiring the introduction of additional Bessel functions or even making the use of this method impossible^[11] (Fig. 4).

In order to use eq. 2, the momentum flowing along each propagator in a diagram must be a linear combination of no more than two of the loop and external momenta^[12]. When the expansion is performed in configuration space this constraint is removed since the propagator then depends only on the distance between the vertices it connects. In addition, if more than three independent momenta are involved, integrals of the form

$$\int d\Omega_b C_{m_1}^\lambda(\hat{a}_1 \cdot \hat{b}) C_{m_2}^\lambda(\hat{a}_2 \cdot \hat{b}) C_{m_3}^\lambda(\hat{a}_3 \cdot \hat{b})$$

may result and the orthogonality relation may not be sufficient to perform all of the angular integrations.

This technique may be applied to calculations involving massive particles. An expansion analogous to Eq. 2 may be derived for a massive propagator. With $n=4$, this approach has been used to calculate many diagrams contributing to the electron magnetic moment to $O(\alpha^3)$ ^[12]. Alternatively it may be possible to calculate massive integrals by expanding each propagator in a Taylor series around $m=0$

$$\frac{1}{(p^2 - m^2)} = \sum_{j=0}^{\infty} \frac{m^{2j}}{[p^2]^{j+1}}$$

and then using Eq. 2. Mass singularities will be transformed into poles in ϵ and the finite power corrections will remain. Even if the resulting sums cannot be performed exactly, the lowest terms in the series may be used to find the leading corrections when the masses are small.

Finally, Eq. 2 with $n=4$ ($\lambda=1$) has been used for several calculations. The photon renormalization constant has been calculated to $O(\alpha^3)$ ¹. It has also been applied to the calculation of the hyperfine splitting in positronium¹³.

I gratefully acknowledge discussions with J. A. Harvey, D. B. Reiss and especially S. Wolfram.

References

1. J. L. Rosner, Ann. Phys. (N.Y.) 44, 11 (1967).
2. M. Dine and J. Sapirstein, Phys. Rev. Lett. 43, 668 (1979);
K. G. Chetyrkin, A. L. Kataev and F. V. Tkachov, Institute for Nuclear
Research (Moscow), preprint (1979), W. Celmaster and R. Gonsalves
UCSD-10P10-206.
3. J. G. Taylor, Gauge Theories of Weak Interactions, Cambridge 1976.
4. W. Kummer, Acta Phys. Austriaca 41, 315 (1975).
5. A. Andrasi and J. C. Taylor, Nucl. Phys. B154, 111 (1979).
6. R. K. Ellis, H. George, M. Machacek, H. D. Politzer, G. G. Ross, Nucl.
Phys. B78, 281 (1978).
7. G.'t Hooft and M. Veltman, Nucl. Phys. B44, 189 (1972).
8. See e.g. R. Barbieri, J. A. Mignaco, and E. Remiddi, Nuovo Cimento 11,
824 (1972) Appendix B.
9. W. Celmaster and R. Gonsalves, UCSD preprint No. UCSD-10P10-207.
10. Erdelyi et al, Higher Transcendental Functions, McGraw-Hill (1955).
11. K. G. Chetyrkin and F. V. Tkachov, Institute for Nuclear Research
(Moscow), preprint (1979).
12. M. Levine and R. Roskies, Phys. Rev. D9, 421 (1974); M. Levine, R. Perisho
and R. Roskies, Phys. Rev. D13, 997 (1976).
13. V. K. Cung, A. Deveto, T. Fulton and W. Repko, Phys. Rev. D18, 3893 (1978).

Footnotes

1. The photon renormalization constant in QED has been calculated to $O(\alpha^3)$ without evaluating a single divergent integral [1]. The analogous QCD calculation - the e^+e^- total cross-section to $O(\alpha_s^2)$ - cannot be so simplified [2].
2. As in all Feynman integrations, a rotation to Euclidean space is tacitly performed.
3. After this work was completed, I learned of similar results obtained by W. Celmaster and R. Gonsalves. They have found eq. 2 with $\rho = 1$ and $\rho = 1 + \epsilon$ to $O(\epsilon)$.
4. Such exponents arise from sub-integrations which can be performed using Eq. 1. The scalar diagram in Fig. 4 is proportional to

$$\Gamma^2(\epsilon) \int d^n p d^n q \frac{1}{[p^2]^{2+\epsilon} (p-k)^2 (p-q)^2 [(q-k)^2]^{2+\epsilon} q^2}$$

TABLE 1

Orthogonality relation:

$$\int d\Omega_b C_{j_1}^\lambda(\hat{a} \cdot \hat{b}) C_{j_2}^\lambda(\hat{b} \cdot \hat{c}) = \delta_{j_1 j_2} \frac{2\pi^{\lambda+1}}{\Gamma(\lambda+1)} \frac{\lambda}{j_1 + \lambda} C_{j_1}^\lambda(\hat{a} \cdot \hat{c})$$

Special Cases:

$$C_0^\lambda(x) = 1 \quad C_1^\lambda(x) = 2\lambda x \quad C_j^\lambda(1) = \frac{\Gamma(j+2\lambda)}{j! \Gamma(2\lambda)}$$

Clebsch-Gordon series

$$C^\lambda(x) C_m^\lambda(x) = \sum_{n=|l-m|}^{l+m} \frac{n! (n+\lambda) \Gamma(g+2\lambda)}{\Gamma^2(\lambda) \Gamma(g+\lambda+1) \Gamma(n+2\lambda)} \frac{\Gamma(g-l+\lambda) \Gamma(g-m+\lambda) \Gamma(g-n+\lambda)}{\Gamma(g-l+1) \Gamma(g-m+1) \Gamma(g-n+1)} C_n^\lambda(x)$$

where $l+m+n = 2g$ and $g = \text{integer}$

Recursion relation

$$(j+1) C_{j+1}^\lambda(x) = 2(j+\lambda) x C_j^\lambda(x) - (j+2\lambda-1) C_{j-1}^\lambda(x)$$

Generating function

$$(t^2 - 2tx + 1)^{-\lambda} = \sum_{j=0}^{\infty} t^j C_j^\lambda(x)$$

TABLE 2

$$x^m = \frac{\Gamma(\lambda)m!}{2^m} \sum_{j=0}^{\lfloor \frac{m}{2} \rfloor} \frac{m-2j+\lambda}{j! \Gamma(1+\lambda+m-j)} C_{m-2j}^\lambda(x)$$

$$e^{ip \cdot x} = \Gamma(\lambda) \left(\frac{|p||x|}{2} \right)^{-\lambda} \sum_{j=0}^{\infty} i^j (j+\lambda) J_{\lambda+j}(|p||x|) C_j^\lambda(\hat{p} \cdot \hat{x})$$

$$(1-ax)^{-\rho} = \frac{\Gamma(\lambda)}{\Gamma(\rho)} \sum_{j=0}^{\infty} \frac{(j+\lambda)\Gamma(j+\rho)}{\Gamma(1+\lambda+j)} \left(\frac{a}{2}\right)^j {}_2F_1\left(\frac{\rho+j}{2}, \frac{\rho+j+1}{2}; \lambda+j+1; a^2\right) C_j^\lambda(x)$$

$$(a^2-2abx+b^2)^{-\lambda} = (ab)^{-\lambda} \sum_{j=0}^{\infty} [T(a,b)]^{j+\lambda} C_j^\lambda(x)$$

$$(a^2-2abx+b^2)^{-\rho} = (ab)^{-\rho} \frac{\Gamma(\lambda)}{\Gamma(\rho)} \sum_{j=0}^{\infty} \frac{(j+\lambda)\Gamma(j+\rho)}{\Gamma(\lambda+j+1)} T(a,b)^{j+\rho} \\ \times {}_2F_1(\rho-\lambda, \rho+j; \lambda+j+1; [T(a,b)]^2) C_j^\lambda(x)$$

Table and Figure Captions

Table 1

Properties of Gegenbauer polynomials. The notation $\int d\Omega_{\hat{b}}$ denotes integration over all directions of the vector \hat{b} .

Table 2

Gegenbauer series. The third formula is derived by expanding $(1-ax)^{-\rho}$ in a binomial series and using the first formula. The last two formulas are found from the third by making a quadratic transformation of the ${}_2F_1$.

Figure 2

These diagrams have been evaluated with several different invariant numerators.

Figure 3

Diagram (a) is in momentum space, while (b) is the same diagram in configuration space.

Figure 4

This diagram cannot be done by Gegenbauer expansion in configuration space.

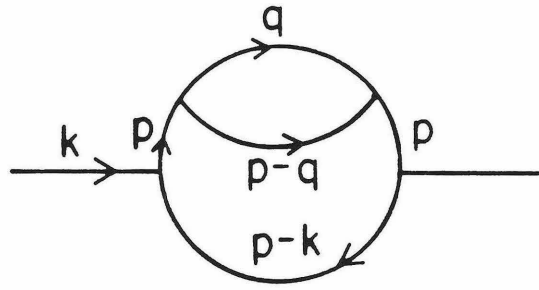


FIGURE 1

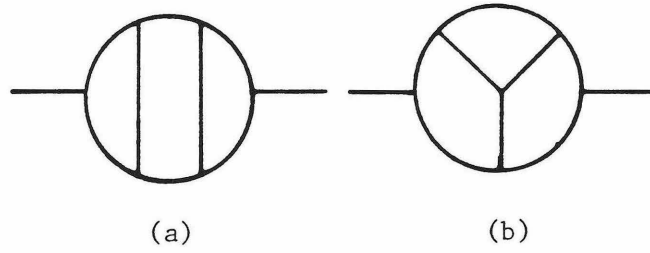


FIGURE 2

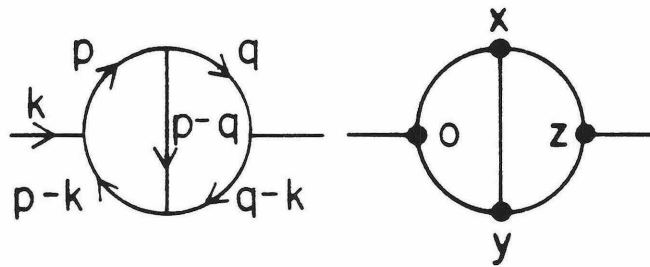


FIGURE 3

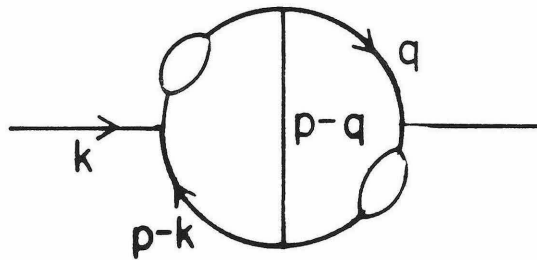


FIGURE 4

Appendix

Gamma Matrix Algebra Program (GAMALG).

written by
Anthony E Terrano (TRES)
and Stephen Wolfram (SWOLF)

mostly on [Feb 25, Mar 3], 1979
revised July 10, 1979.

Capabilities:

- [1] Takes traces of products of Dirac gamma matrices in n dimensions. In 4 dimensions, it also takes traces of products involving gamma[5] (G5). The results may have free indices.
- [2] Squares sums of amplitudes, involving polarized or unpolarized spinors.
- [3] Contracts free indices.
- [4] Simplifies products of gamma matrices in n dimensions.

For all manipulations, GAMALG uses the conventions of Bjorken and Drell and takes $\text{Tr}(1)=4$ (generalization of the spinor dimensionality is unnecessary).

Further information, especially on the algorithms used by GAMALG, may be found in 'MACSYMA Tools for Feynman Diagram Calculations', by Stephen Wolfram, in Proceeding of the 1979 Users' Conf. and Caltech preprint CALT-68-720 (June 1979). These references give some discussion of other programs available for high energy physics calculations (including Feynman parametrization etc.).

Summary of Functions:

[sections under which functions discussed given in brackets] (Note: in all functions taking a string of arguments (e.g. TR), list brackets ([,]) may be included or omitted as desired.)

BTR(list) takes the trace of the gamma matrices represented by its argument in a way that is more efficient than TR for long traces involving many sums of momenta [1].

CIND(mu1,...,muk) adds mu1 through muk to the list of contracted indices [1].

CGT(exp) converts G's to TR's and does them [3].

COMPDEF(vec1=list1,vec2=list2,ind1=val1,ind2=val2,vec3=...) defines lists as the components of vectors and values for indices, for use by NON-COV

CON(exp) contracts all free indices in *exp* (including epsilon symbols) [3].

CONJ(amp) returns the conjugate of the amplitude *amp* [2].

COTR(exp) reduces (in $n=4$) products of traces with contracted indices to single traces [3].

CRUNCH(exp) simplifies untraced products of gamma matrices in *exp* [3].

DFIX(exp) expands all dot products in *exp* [3].

EPSFIX(exp) expands all epsilon symbols in *exp* [3].

FLAGS() displays the values of flags and information lists.

GFIX(exp) expands sums of vectors appearing in untraced products of gamma matrices in *exp* [3].

GLUE3(i1,i2,i3) gives the tensor corresponding to the three-gluon vertex represented by its arguments [3].

KINDEF(dotp1=rep1,dotp2=rep2,...) defines kinematics substitutions *dotp1=rep1,...* [3].

NONCOV(exp) substitutes the non-covariant components specified by **COMPDEF** for vectors and indices in dot products in *exp* [3]

NSET(dim) sets the dimensionality of spacetime to *dim* [1].

SCALS(x1,...,xk) adds *x1* through *xk* to the list of scalars [1].

SQ(spn1,amp,spn2) squares the amplitude *amp* sandwiched between the spinors *spn1* and *spn2* [2].

SQAM(spn1,amp1,spn2,amp2) sums over spins the amplitude squared *amp1*conj(amp2)* sandwiched between the spinors *spn1* and *spn2* [2].

TR(a1,a2,...) takes the trace of gamma matrices represented by its argument [1].

UNCIND(mu1,...,muk) removes *mu1* through *muk* from the list of contracted indices [1].

UNCOMPDEF(vec1,ind1,vec2,vec3,...) removes the components defined for its arguments [3].

UNKINDEF(dotp1,...,dotpk) removes simplifications defined for dot products *dotp1* through *dotpk* [3].

UNSCALS(x1,...,xk) removes *x1* through *xk* from the list of scalars [2].